Research Square

Preprints are preliminary reports that have not undergone peer review.
They should not be considered conclusive, used to inform clinical practice,
or referenced by the media as validated information.

Clonally selected hypoimmune limbal stem cells: an in vitro proof-of- concept towards an off-the-shelf therapy for limbal stem cell deficiency

Eldo Galo
Newcastle University
Sean Hockney
Newcastle University
Kaltra Mezini
Newcastle University
Graham R. Smith
Newcastle University
Birthe Dorgau
Newcastle University
Michael McCorkindale
Newcastle University
Simi Ali
Newcastle University
Francisco C. Figueiredo
Royal Victoria Infirmary
Majlinda Lako
majlinda.lako@ncl.ac.uk
Newcastle University
Lyle Armstrong
Newcastle University

Research Article

Keywords:

Posted Date: October 30th, 2026

DOI: https://doi.org/10.21203/rs.3.rs-11142612/v1

License: This work is licensed under a Creative Commons Attribution 4.0 International License.
Read Full License

Additional Declarations: No competing interests reported.

Clonally selected hypoimmune limbal stem cells: an *in vitro* proof-of-concept towards an off-the-shelf therapy for limbal stem cell deficiency

Eldo Galo [1], Sean Hockney [1], Kaltra Mezini [1], Graham R. Smith [2], Birthe Dorgau [1], Michael McCorkindale [2], Simi Ali [3], Francisco C. Figueiredo [1,4,] Majlinda Lako [1#,] Lyle Armstrong [1#]

1. Biosciences Institute, Newcastle University, Newcastle upon Tyne, UK
2. Bioinformatics Support Unit, Newcastle University, Newcastle upon Tyne, UK
3. Clinical and Translational Research Institute, Newcastle University, Newcastle upon Tyne, UK
4. Ophthalmology, Royal Victoria Infirmary, Newcastle Hospitals NHS Foundation Trust, Newcastle Upon Tyne, UK.

to whom the correspondence should be addressed

Prof. Lyle Armstrong or Prof. Majlinda Lako
Biosciences Institute
Newcastle University
International Centre for Life
Central Parkway
Newcastle NE1 3BZ

Email: lyle.armstrong@ncl.ac.uk or majlinda.lako@ncl.ac.uk

Abstract

Limbal stem cell deficiency (LSCD), a highly morbid and uncomfortable condition, causes progressive corneal opacification and vision loss through irreversible loss of the limbal epithelial stem cell pool. Current transplantation strategies are limited by significant challenges across both autologous and allogeneic approaches: allogeneic grafts require long-term systemic immunosuppression and carry poor long-term survival, while even autologous transplants, free from rejection, suffer approximately one-third graft failure, partially attributable to donor variability. Here, we report the generation of hypoimmune limbal stem cells (LSCs) engineered to evade allogeneic immune recognition while retaining full stem cell identity and differentiation competence. Using ROCK inhibitor-supported long-term culture, we demonstrate stable LSC expansion exceeding 202 population doublings, with preserved transcriptomic identity and differentiation capacity. Simultaneous CRISPR-Cas9-mediated knockout of *B2M* and *CIITA*, combined with lentiviral CD47 overexpression, conferred complete *in vitro* evasion of $CD4^+$ and $CD8^+$ T cell responses and abrogated macrophage-mediated phagocytosis. These findings establish an *in vitro* proof-of-concept framework towards a universal, off-the-shelf allogeneic LSC product that eliminates the need for systemic immunosuppression and reduces donor-dependent variability, with broad implications for the scalable treatment of both unilateral and bilateral LSCD.

Introduction

Corneal clarity and function rely on the perpetual renewal of its epithelium. This self-renewing ability is maintained throughout life by limbal stem cells (LSCs), which reside in the limbal niche at the corneoscleral junction [1,2]. In addition to providing new corneal epithelial cells, LSCs also act as a barrier that prevents the encroachment of conjunctival epithelium and associated stromal vasculature into the normally avascular and transparent cornea [3].

Loss or damage to LSCs and/or interference with their supportive LSC niche results in limbal stem cell deficiency (LSCD). LSCD is characterised by conjunctivalisation of the corneal surface and hallmark signs of epithelial instability, including neovascularisation, inflammation, scarring, and opacity. These changes lead to visual impairment and distressing symptoms such as pain, photophobia, and excessive tearing [4]. Management of LSCD focuses on restoring a healthy ocular surface and reconstructing the limbal niche to support the existing or transplanted LSCs [5].

Over the past three decades, several autologous and allogenic cell-based and surgical approaches have been applied to restore severely damaged or diseased ocular surface epithelium, including direct grafting of harvested tissue (simple limbal epithelial transplantation (SLET) [6], conjunctival limbal autograft/allograft (CLAU/CLAL) [7,8], cadaveric keratolimbal allograft (KLAL)) [8-10] and cultivated limbal epithelial transplantation (CLET) [11-14]. In unilateral LSCD, autologous transplantation represents

the gold-standard approach [15]. Limbus-derived tissue from the contralateral healthy eye is either directly transplanted using SLET or CLAU techniques or expanded ex vivo to produce an LSC sheet subsequently grafted onto the affected cornea (CLET). In contrast, patients with bilateral LSCD must rely on allogeneic tissue sources or ex vivo expansion of autologous oral mucosa epithelial stem cells [16], which do not fully transdifferentiate into corneal epithelium.

Compared with allogeneic grafting, autologous grafting offers greater efficacy, reduced complications, and eliminates the risk of immune rejection [1,17]. Long-term outcomes of cadaveric allogeneic CLET remain poor (<25% survival beyond three years) despite systemic immunosuppression, whereas autologous grafts achieve up to 76.6% success at ten years [14,18]. The failure of autologous grafts is not attributed to rejection, but rather to factors such as donor variability, permanent destruction of the LSC niche and the inflamed host graft bed [19-21].

Both autologous and allogeneic limbal transplants involve harvesting of healthy limbal tissue; however, variability in cell sources and personalised manufacturing protocols can result in inconsistent therapeutic outcomes. Notably, there is often a delay between tissue retrieval and transplantation, meaning that immediate availability of transplant-ready tissue is not possible [15]. Hence, there is a clear and significant unmet need for a cost-effective, clinically applicable, and above all, “off-the-shelf” source of LSCs for the treatment of both uni- and bilateral LSCD [22].

To achieve this goal, several teams have pioneered the concept of genetically engineering allogeneic cells, enabling them to evade recognition by the host's innate and adaptive immune system [23-28]. Remarkably, these studies have demonstrated that just three targeted modifications, namely the depletion of HLA class I and class II molecules through knockout of *B2M* and *CIITA*, respectively, combined with overexpression of CD47, were sufficient to achieve complete immune invisibility, as confirmed by extensive *in vitro* analyses[24-26]. This strategy has demonstrated preclinical success in allogeneic iPSC derivatives and shown safety and tolerability in phase I clinical trials using primary β-islets for the treatment of type 1 diabetes [29], as well as in CAR-T cell therapies [30] for refractory B-cell malignancies.

Importantly, the concept of hypoimmunogenicity could be applied to any transplantable human stem cell type, including LSCs, provided that appropriate culture conditions exist for prolonged *ex vivo* expansion to facilitate gene editing. Currently, *ex vivo* protocols for LSC culture do not fully replicate the native limbal niche, resulting in suboptimal long-term maintenance of these cells. Combining a Rho-associated kinase (ROCK) inhibitor (Y-27632) with the classical 3T3-J2 mouse embryonic fibroblast feeder layer has been shown to support extended LSC growth *in vitro*[31-34]. Several studies have reported that this culture system enables the long-term maintenance of LSCs *ex vivo*; however, it remains uncertain whether these cells fully retain their native phenotype and functional identity.

Herein, we present a comprehensive comparative analysis of human LSCs cultured with or without ROCK inhibitor Y-27632 (Ri). Our results demonstrate that LSCs maintained

under R+ conditions preserve their transcriptional profile, proliferative potential exceeding 202 population doublings (PD), and differentiation capacity across extended passages. Subsequently, we employed CRISPR-Cas9 genome editing combined with lentiviral vector delivery to generate clonal hypoimmunogenic LSCs (LSC B2M$^{-/-}$CIITA$^{-/-}$ CD47OE). These engineered cells exhibited effective immune evasion *in vitro*, as evidenced by significantly diminished activation of allogeneic immune cells in co-culture assays and resistance to macrophage-mediated phagocytosis.

Results

Rock Inhibitor enables scalable human LSC expansion and promotes stemness while preserving transcriptional identity and differentiation potential throughout serial passages

LSCs were isolated from three adult human eyes using enzymatic digestion as described in the methods section. The isolated LSCs were expanded in culture for two passages to generate sufficient cell stocks. Early-passage LSCs were thawed and used as the experimental starting material, then passaged at semi-confluency in the presence (R+) or absence (R-) of Ri. Throughout the passages, R- and R+ cultures were evaluated for cell morphology, colony-forming efficiency (CFE), PD, differentiation capacity, proliferative capacity, and wound-healing ability. Additionally, samples were collected for bulk RNA-seq transcriptomic profiling.

While untreated LSCs became senescent and ceased proliferation after 6-8 passages, R+ LSCs maintained their characteristic epithelial cobblestone morphology (**Fig. S1A)** and proliferative capacity beyond passage 35 **(Fig. S1B),** corresponding to more than 202 (±6.8) PDs. R+ cells exhibited a higher proliferation rate, reaching semi-confluency in an average of 7.4 (±0.93) days per passage, compared to approximately 10.5 (±2.08) days for R- cells (**Fig. S1B**). This increased proliferative capacity was supported by colony-forming CFE assays (**Fig. S1C**) and flow cytometric quantification of $Ki67^+$ proliferative cells (**Fig. S1D**), both of which declined in R- but were preserved in R+ LSCs. Given the critical role of LSC migration and proliferation in corneal epithelial wound healing, we assessed scratch assay wound closure dynamics. R+ cultures achieved complete closure by 27 hours (±6.4 h), whereas R- cultures healed only ~51.1% (±15.6%) at the same time point (**Fig. S1E**).

Bulk RNA-seq was performed on R- (P3-P7) and R+ (P4-P14) LSCs and their air-liquid interface differentiated (ALI) derivatives (R-: ALI-P3, ALI-P4, ALI-P6, R+: ALI-P4, ALI-P6, ALI-P12) **(Fig. 1A)**. The PCA plot clusters the samples according to their similarity and shows little variability among triplicates. 75.7% of the variability is explained by PC1 and only 10.11% by PC2. The plot separates into two distinct halves, with LSCs from all samples located on the left and ALI-differentiated samples on the right, indicating that PC1 (75.7%) captures the variability associated with the transition from the stem cell to the differentiated state. The initial P3 (iP3) sample is located in proximity to both early passage R+ LSCs (P4-P6) and early passage R- LSCs (P4-P7) groups. Within the early passage (R-) group of LSCs, as the passage number increases, a trend toward differentiation is observed. iP3, early passage R+ LSCs, transitory R+ LSCs and late

passage R+ LSCs seem to be similar in PC1 but variable in PC2. With increasing passage number in R+ cells, both LSCs and ALI-differentiated cells progressively shift upward toward higher PC2 values in the PCA plot **(Fig. 1A)**. Reflective of the PCA plot, the Pearson correlation coefficient (r) between the clusters shows that when R+ and R- clusters are compared to the iP3, all three R+ clusters (early p. R+, transitory & late p. R+) show a higher correlation (r= 0.87-0.89) to iP3 than the R- LSCs (r=0.79). A strong correlation is observed between all R+ treated samples (r= 0.97-0.98), indicating high similarity and stability in gene expression throughout passages. Moreover, R- LSCs were more strongly correlated with the ALI-differentiated cluster (r = 0.75), whereas R+ samples and iP3 displayed only moderate correlations (r = 0.51–0.55) (Fig. 1B) **(Fig. 1B)**.

To ascertain whether LSCs maintain their identity when exposed to Ri over successive passages, we constructed a heatmap using candidate markers selected from relevant literature, particularly those employed in characterising LSCs in single-cell transcriptomics investigations [35,36]. Inspection of the heatmap indicates that most stem cell/progenitor markers maintain a stable expression pattern across LSC samples. R+ LSCs maintain expression levels akin to iP3 throughout the passages, whereas expression of these markers in R- LSC samples tends to gradually decrease while the passage number increases **(Fig. 1C)**. At passage 7, the expression of the stem cell markers in R- LSCs is low and comparable to that observed in ALI differentiated samples. The low levels of these markers in the ALI differentiated samples align with prior literature [35,36] and suggest that proliferation and stem cell phenotypes are arrested in these differentiated states. Expression of the LSC/progenitor markers is absent in both R+ and R- ALI differentiated samples **(Fig. 1C)**.

Late R+ LSCs (P11, P12, P13, P14) show increased expression of markers enriched in basal epithelial cells, such as *GJB1*, *GJB2*, *GJB6* and *BMP7*, a secreted ligand of the TGF-beta receptor family. Moreover, putative limbal markers such as the transcription factor *TP63*, calcium binding protein *S100A2*, chemokine ligand *CXCL14*, ATPase Na+/K+ Transporting protein *ATP1A1*, basal limbal epithelial marker *KRT14*, and basal limbal and corneal epithelial marker *KRT5* show the same pattern of increased expression with time in culture **(Fig. 1C)**. As one of the best-characterised putative markers of LSCs, whose high expression is associated with improved graft success (Rama et al., 2010), *TP63* expression levels were validated by qPCR. *TP63* expression was significantly higher in R+ LSCs compared with R- LSCs. Moreover, *TP63* expression was further increased in late-passage R+ LSCs **(Fig. 1D)**. To validate these transcriptomic findings, we performed immunofluorescence analysis using KRT15 and p63 antibodies. These markers were first validated in human limbal and central corneal sections, where they localised to the basal limbal layer but were absent from the central cornea. In contrast, differentiated epithelial markers KRT3 and KRT12 were expressed in the suprabasal layers of the central cornea (**Fig. S2A**), but were absent from the limbus (data not shown). Immunofluorescence analysis using these validated antibodies showed that p63 expression patterns in R+ and R- limbal stem cells closely mirrored results from bulk RNA sequencing and qPCR across successive passages **(Fig. S2B)**.

The ALI differentiation method did not induce *KRT12* expression, and *KRT3* expression remained minimal in cultures derived from both R- and R+ conditions. Additionally, markers reported to be expressed in corneal suprabasal and superficial cells, such as

KRT24, HES5, HES1, and *AREG*, were not detected in differentiated samples from either culture condition (**Fig. 1C)**. Although ALI differentiated cells express the previously mentioned markers at low levels, they robustly express markers characteristic of superficial corneal and conjunctival epithelium, including *MUC1, MUC16,* and *MUC4*. Additionally, markers typically found in wing cells of the central cornea, such as *CXCL17*, and the limbal superficial epithelium marker *LYPD2*, are present. Notably, these markers exhibit higher expression in both ALI differentiated cells and R- limbal stem cell cultures compared to R+ LSCs. The same trend was observed for *RHOV* and *CLDN7*, both markers of post-mitotic and terminally differentiated migratory epithelial cells. Nevertheless, no significant differences were observed in the expression patterns of ALI differentiated cultures derived from R+ and R- treated cells demonstrating that long term expansion of LSCs in the presence of R+ does not affect their differentiation potential **(Fig. 1C)**. The above-mentioned markers are expressed in iP3 and persist in early R-; some are also present in early R+ cultures, only to result in a decrease of expression in Late R+ LSCs. This decrease of differentiation markers from iP3 to later passages of R+ LSCs, accompanied by the increase in the stem/progenitor cell marker expression, reveals a heterogeneous population of cells in the early passages and an enrichment in the LSC population throughout the passages in R+ LSCs **(Fig. 1C)**.

Taken together, these findings suggest that Ri enables scalable *ex vivo* LSC expansion while preserving stem cell identity and differentiation capacity.

Immunomodulatory Surface Ligand Characterisation in LSCs and ALI-derivatives

To gain insight into the immunological properties of LSCs and their ALI differentiated derivatives under normal and inflammatory (IFN-γ treated) conditions, we characterised the surface expression of a panel of ligands with established roles in immune recognition and modulation using flow cytometry. These included classical antigen-presentation molecules (HLA-I A/B/C, HLA-II DP/DR/DQ), non-classical immunomodulatory HLA molecules (HLA-G, HLA-E), innate immune checkpoint ligands (CD47, PD-L1), and co-stimulatory or adhesion molecules (CD40, ICAM, CD80, CD86). Characterising the expression profiles between LSCs and their ALI-derivatives in normal and inflammatory conditions provides critical insight into their immunogenicity and interactions with host immune cells.

These markers play pivotal roles in cellular recognition. HLA-I (A, B, C) presents endogenous peptides to cytotoxic CD8+ T cells for direct alloreactive recognition [37], while non-classical HLA-G and HLA-E engage inhibitory KIRs on NK cells [38,39] and ILT2/ILT4 receptors on macrophages [40]. HLA-II (DP, DR, DQ) presents antigens to CD4+ T cells; its upregulation drives direct alloresponses that promote alloantibody production and accelerate rejection [41-43]. CD47 delivers a "don't-eat-me" signal via SIRPα on macrophages and dendritic cells, suppressing phagocytosis, antigen uptake, and the downstream T-cell activation cascade [44]. It also inhibits NK cell-mediated lysis [26]. PD-L1 engages PD-1 on activated T cells to induce exhaustion[45]; it further reduces phagocytosis by PD-1^{+} macrophages [46] and cytotoxicity by PD-1^{+} NK cells [25]. CD80/CD86 provide CD28-mediated costimulation to T cells or, with higher affinity, suppress them via CTLA-4 engagement [47]. CD40 delivers activation/maturation signals to antigen-presenting cells (APCs) via the CD40-CD40L axis, enabling full functionality

and antigen cross-presentation. CD40 expression on epithelial cells has been linked to the development of inflammatory conditions, induction of self-tolerance, and allograft rejection [48]. ICAM-1 mediates adhesion of leukocytes, facilitating immune synapse formation [49].

At baseline, both LSCs and ALI-derived cells uniformly expressed HLA-I, which was further upregulated by IFN-γ (MFI) to a similar extent in both populations (**Fig. S3A**). In contrast, HLA-II was more prevalent in ALI cells at baseline (24.6% vs 2.3% in LSCs), but IFN-γ induced near-universal expression in both populations (LSCs 98.8%, ALI 86.6%) with comparable expression levels (**Fig. S3B**). HLA-G was detected in only small fractions of cells (LSCs 3.2%, ALI 7.5%) and remained unchanged following stimulation, with similar expression levels in both groups (**Fig. S3C**). HLA-E was absent at baseline but induced by IFN-γ, more prominently in LSCs (93.1%) than ALI cells (46.1%), although expression levels per positive cell were comparable (**Fig. S3D)**.

CD47 was uniformly expressed at baseline and significantly upregulated following IFN-γ without significant differences between populations (**Fig. S3E**). PD-L1 expression increased markedly after stimulation in both LSCs (61.1% to 99.4%) and ALI cells (67.7% to 95.8%), with similar expression levels across conditions (**Fig. S3F**). ICAM-1 and CD40 were both induced by IFN-γ in LSCs and ALI cells; however, LSCs showed higher proportions of positive cells (ICAM-1: 94.4% vs 51.9%; CD40: 85.9% vs 43.3%), whereas ALI-derived cells exhibited higher expression levels per positive cell (**Fig. S3G–H**). CD86 was absent in LSCs but present in a subset of ALI cells (17.7%) and was not modulated by IFN-γ (**Fig. S3I**), while CD80 was not detected under any condition (**Fig. S3J**).

We also characterised the expression pattern of T and NK cells activating and inhibitory ligands, which demonstrated that LSCs and ALI-derived cells exhibit distinct immuno-ligand expression profiles (**Fig. S4A, B**). LSCs showed passage-dependent expression of T cell inhibitory ligands, with *PVR, PD-L2, CD276*, and *NECTIN3* predominating in early passages and *VISTA* increasing at later passages (**Fig. S4A**). They exhibited a restrained T cell activating repertoire limited to *HLA-G, CD30L*, and *GITRL*, and NK inhibitory ligand expression dominated by adhesion molecules (*NECTIN1, CDH2, CDH4, COL1A1*) alongside passage-dependent *HLA-G* and *NECTIN3*. ALI-differentiated cells displayed upregulated T cell co-stimulatory ligand expression, including *HLA class I* and *II*, *4-1BB-L, CD27L, CD40, TNFSF14, HVEM*, and butyrophilins, alongside NK inhibitory ligands centred on HLA class I molecules and *CD47*, and T cell checkpoint ligands including *PD-L1, LGALS9, NECTIN*2, and *VSIG3*. Notably, NKG2D ligands (*RAET1L, ULBP1, RAET1E, RAET1G, CADM1*) were more highly expressed in LSCs (**Fig. S4A, B**).

Taken together, these data reveal distinct immunomodulatory profiles between LSCs and their ALI-differentiated derivatives, shaped by differentiation state and amplified under inflammatory conditions. LSCs exhibit a stem-like immune signature characterised by higher baseline CD40, inducible HLA-E, and restrained HLA-II and ICAM-1 expression. In contrast, ALI-derived cells display more mature epithelial characteristics, with elevated baseline HLA-II, CD86, and ICAM-1 potentially conferring increased adaptive immune interaction and retention. These findings suggest that differentiation state critically shapes how limbal epithelial stem cell grafts are perceived and engaged by host immune effectors in both steady-state and inflammatory environments.

Engineering HLA-I and HLA-II ablated LSCs

Developing successful hypoimmune cell therapies requires the ablation or downregulation of cell-surface HLA Class I and II molecules. We achieved this by inactivating *B2M* and *CIITA*, the primary genetic regulators of HLA-I and HLA-II expression. Utilising the CRISPR/Cas9 system, we introduced targeted indels within exon 2 of *B2M* and exon 3 of *CIITA* (**Fig. 2A, B**). This dual-knockout strategy was implemented in early-passage LSCs via the simultaneous delivery of ribonucleoprotein (RNP) complexes, facilitating the efficient disruption of antigen presentation pathways. Following nucleofection, LSCs were expanded to semi-confluence on feeder-coated plates. To validate the double knockouts, the cell pool was stimulated with IFN-γ to induce HLA-I and II expression. The resulting HLA-I^-/HLA-II^- double-negative fraction was then isolated via single-cell sorting into 96-well plates containing LSC conditioned medium and Ri for clonal expansion (**Fig. 2A**).

Flow cytometric analysis of the nucleofected LSC pool identified four distinct populations based on HLA surface expression (**Fig. 2C**). The double-negative fraction (HLA-I^-/HLA-II^-, Population 4) accounted for 32.1% of the pool, indicating successful simultaneous disruption of both *B2M* and *CIITA*. We also identified a double-positive population (HLA-I^+/HLA-II^+, 16.3%) representing either wild-type or partially edited cells, and two intermediate populations exhibiting single-locus loss: HLA-I^-/HLA-II^+ (Population 7, 10.4%) and HLA-I^+/HLA-II^- (Population 6, 19.3%).

Following clonal expansion of the double-negative fraction, genomic DNA was extracted to verify indel formation. We employed a PCR-based screening strategy where primers were designed to anneal directly across the sgRNA cleavage sites; consequently, successful indel formation prevented primer binding and abolished amplification (**Fig. 2D**). All selected clones (12, 13, 16, and 18) were confirmed to harbour biallelic disruptions in both *B2M* and *CIITA*. Confirmatory flow cytometry further demonstrated the complete ablation of HLA-I and HLA-II surface expression (**Fig. 2E**).

Among the validated $B2M^{-/-}CIITA^{-/-}$ clones, Clone 13 (c13) was selected for further study as it exhibited superior LSC-characteristic morphology (**Fig. 2F**) and a significantly higher CFE (**Fig. 2G**). Sanger sequencing of the target regions in c13 confirmed the presence of frameshift mutations, ensuring stable functional knockouts (**Fig. 2H**). To ensure genomic integrity, c13 was screened for predicted CRISPR/Cas9 off-target effects. Analysis of loci containing up to three mismatches revealed no detectable modifications, confirming the high specificity of the dual-editing approach (**Fig. S5**).

Overexpression of the CD47 immune checkpoint inhibitor in HLA-I and HLA-II ablated LSCs

CD47 acts as a critical inhibitory "self-signalling" molecule by engaging the immune receptor SIRPα, which effectively suppresses phagocytosis [50]. SIRPα is predominantly expressed on myeloid lineage cells with phagocytic capacity, including macrophages, dendritic cells, granulocytes, and monocytes, and is also present on Natural Killer (NK)

cells [51]. Recent evidence suggests that the overexpression of CD47 in HLA-I/II-deficient K-562 cells provides a dual layer of protection, shielding them from both macrophage-mediated phagocytosis and NK cell-mediated "missing-self" cytotoxicity [25]. Notably, data from HLA-I/II-ablated primary human islets and iPSCs suggest that CD47-mediated NK cell inhibition is threshold-dependent, with quantitative flow cytometry demonstrating that a minimum of approximately 184,773–203,853 antibody binding capacity units per cell (ABC) is required to confer effective protection [25].

To mitigate "missing-self" triggered cytotoxicity in HLA-I/II ablated LSCs, a lentiviral vector (LV-CD47) was utilised to enforce CD47 expression under the control of the *EF-1α* promoter (**Fig. 3A**). We established an optimal multiplicity of infection (MOI) of 4 using a control mCherry lentiviral vector (**Fig. S6A-C**). LSC $B2M^{-/-}CIITA^{-/-}$ (c13) LSCs were transduced in suspension and subsequently plated on blasticidin-resistant feeder layers. At 72 hours post-transduction, we initiated selection with 6 ug/ml blasticidin, followed by the isolation of the $CD47^{Bright}$ population via single-cell sorting into 96-well plates (**Fig. 3B**).

To confirm sorting efficiency, we analysed pooled $CD47^{DIM}$, $CD47^{MID}$ and $CD47^{Bright}$ populations. The $CD47^{Bright}$ pool exhibited the highest levels of both transcript and protein expression (**Fig. 3C**). Following clonal expansion, we prioritised the ten clones with the highest *CD47* mRNA expression for further characterisation (**Fig. 3D**). Surface CD47 levels were precisely quantified via quantitative flow cytometry by measuring the ABC per cell (**Fig. 3E; Fig. S6D**). Intriguingly, both WT and $B2M^{-/-}CIITA^{-/-}$ LSCs exhibited high physiological baseline CD47 expression (219,568 and 197,568 ABC, respectively), which

falls within the proposed threshold for NK-cell resistance in islets and iPSCs. Despite these high baseline levels, the engineered CD47-overexpressing LSC clones (LSCs B2M$^{-/-}$CIITA$^{-/-}$CD47OE) demonstrated a substantial 12- to 28.5-fold increase in surface CD47 expression compared to wild-type controls (**Fig. 3E**).

From the generated LSC B2M$^{-/-}$CIITA$^{-/-}$CD47OE candidates, six clones were identified as harbouring three or fewer lentiviral vector copies per genome (**Fig. 3F; Fig. S6E**). These clones underwent further functional screening for CFE. The two top-performing clones, sc17 and sc35, exhibited the highest CFE and were prioritised for downstream characterisation (**Fig. 3G**). To confirm that the extensive genetic engineering (triple knockout/overexpression) did not compromise cellular potency, these lead clones were subjected to ALI differentiation alongside LSC B2M$^{-/-}$CIITA$^{-/-}$. Histological analysis of transwell cross-sections demonstrated the maintenance of the epithelial phenotype. Staining confirmed the robust expression of LSC stem/progenitor cell markers (KRT15, p63) and the successful transition to differentiation markers, including KRT3 and MUC4 (**Fig. 3H**).

These findings demonstrate that simultaneous HLA ablation and CD47 overexpression can be achieved without altering the fundamental biological properties of LSCs.

B2M$^{-/-}$CIITA$^{-/-}$CD47OE LSCs and ALI derivatives avoid T cell recognition and proliferation

Given the differential immunoregulatory ligand expression between LSCs and their ALI-differentiated progeny **(Fig. S3; S4A, B)**, and the highly inflammatory microenvironment that characterises LSCD *in vivo*, we next evaluated the immune evasive properties of generated LSCs (WT, B2M$^{-/-}$CIITA$^{-/-}$ & B2M$^{-/-}$CIITA$^{-/-}$CD47OE clones) and their ALI progeny under inflammatory conditions using a 3-week allogeneic T cell co-culture model. To more faithfully mimic the transplantation setting, co-cultures were performed in the absence of Ri, thereby precluding its potential influence on both target cell immune ligand expression (**Fig. S4C**) and T cell activation [52].

Pan T cells (CD3^{+}) were isolated from PBMCs of four allogeneic human donors by negative MACS, and the corresponding T cell-deprived fraction of PBMCs was retained for use as autologous APCs. LSCs and ALI target cells were preconditioned with IFNγ for 48 hours before co-culture. 8 × 10^{5} CellTrace Violette (CTV) - stained Pan T cells and 2 × 10^{5} of CD3^{-} PBMC fraction were added onto the target cells. To sustain antigen exposure, the cultures were maintained for three weeks through weekly serial passage of the effector cells onto freshly prepared target and CD3^{-} PBMC cells (**Fig. S7A**). T cell activation and proliferation were monitored by flow cytometry at weekly intervals to track the allogeneic response over the 3-week period (**Fig. 4A**). Non-stimulated CD3^{+} and CD3^{-} PBMC cells were used as a baseline, while CD3/CD28 Dynabeads served as a positive control for effector cell activation. The T cell activation and proliferation was assessed by the panel presented in the methods section **(Table S9)**, and the gating strategy is described in **Fig.S8**. Pan T cells were characterised for helper T cell (CD4+) and cytotoxic T cell (CD8+) subsets and within each subset proliferation and activation (CD25+) were assessed. Memory subsets within CD4^{+} and CD8^{+} T cells were defined by CD62L and

CD45RO expression, identifying central memory (TCM/CD45RO$^+$CD62L$^+$) and effector memory (TEM/CD45RO$^+$CD62L$^-$) populations. Proliferation was subsequently analysed within the TCM and TEM fractions of both CD4$^+$ and CD8$^+$ compartments (**Fig.S8**).

At week 1 in both LSC **(Fig. 4A)** and ALI **(Fig. 5A)** co-cultures, we observed no activation or proliferation of CD3$^+$ Pan T cells, CD4$^+$ T helper cells, or CD8$^+$ cytotoxic T cells. And by week 3, the non-specific baseline proliferation masked differences attributable to the target cells, making week 2 the most informative timepoint for comparing the immunogenicity of LSCs and ALI-derived cells. Therefore, the subsequent analysis is focused on this time point.

In LSC co-cultures, more than 88% of live leukocytes (CD45$^+$) were T cells (CD3$^+$). No significant differences were observed between LSC conditions in the proportion of pan T cells **(Fig. 4B)**; however, a significantly higher proportion of proliferating pan T cells was detected in co-cultures with WT LSC **(Fig. 4b)**. T cells co-cultured with B2M$^{-/-}$CIITA$^{-/-}$CD47OE LSCs exhibited proliferation comparable to baseline, whereas B2M$^{-/-}$CIITA$^{-/-}$ LSCs showed a non-significant trend toward increased T cell proliferation **(Fig. 4b)**.

In contrast to the positive control, the proportions of CD4$^+$ **(Fig. 4C)** and CD8$^+$ **(Fig. 4G)** T cells were similar to baseline across all LSC co-cultures, including WT. Although a trend toward higher CD4$^+$ T cell proliferation was observed in WT LSC co-cultures, this did not reach significance **(Fig. 4c)**. Conversely, CD8$^+$ T cell proliferation was significantly elevated in WT LSC co-cultures, whilst co-cultures with B2M$^{-/-}$CIITA$^{-/-}$ and

B2M$^{-/-}$CIITA$^{-/-}$CD47OE LSCs maintained proliferation levels comparable to baseline **(Fig. 4g)**.

A significantly higher proportion of activated CD4^{+}CD25^{+} cells was observed in WT LSC co-cultures, whereas B2M$^{-/-}$CIITA$^{-/-}$CD47OE LSCs yielded CD4^{+}CD25^{+} levels comparable to baseline. B2M$^{-/-}$CIITA$^{-/-}$ co-cultures showed an intermediate trend, with activation higher than both CD47OE clones and baseline **(Fig. 4D)**. This pattern was mirrored in CD4^{+}CD25^{+} proliferation, where B2M$^{-/-}$CIITA$^{-/-}$CD47OE co-cultures exhibited significantly lower proliferation than B2M$^{-/-}$CIITA$^{-/-}$, and WT co-cultures showed significantly greater proliferation than B2M$^{-/-}$CIITA$^{-/-}$co-cultures **(Fig. 4d)**.

Activated CD8^{+}CD25^{+} cells mirrored the activation pattern observed for CD4^{+}CD25^{+} cells across LSC conditions **(Fig. 4H)**, however, no proliferation of CD8^{+}CD25^{+} cells were detected in B2M$^{-/-}$CIITA$^{-/-}$ co-cultures **(Fig. 4h)**. This distinction suggests an initial CD4^{+} T helper cell engagement in B2M$^{-/-}$CIITA$^{-/-}$ LSC co-cultures that occurs predominantly through indirect allorecognition mediated by the APCs present in the CD3^{-} fraction.

The proportions of TCM **(Fig. 4F)** and TEM **(Fig. 4E)** populations within CD4^{+} T cells remained unchanged across all LSC co-culture conditions. However, proliferation of CD4^{+} TEM **(Fig. 4e)** cells was elevated in co-cultures with WT compared to B2M$^{-/-}$CIITA$^{-/-}$ CD47OE LSCs, which displayed proliferation levels identical to the baseline. Proliferation of CD4+ TCM was significantly increased in co-cultures with WT and B2M$^{-/-}$CIITA$^{-/-}$ LSCs compared to B2M$^{-/-}$CIITA$^{-/-}$CD47OE LSCs, which displayed proliferation levels identical to the baseline (**Fig. 4f**).

Within the $CD8^+$ cytotoxic T cell compartment, the TCM **(Fig. 4J)** population was comparable across all LSC co-culture conditions; however, a higher proportion of TEM cells was observed in co-cultures with WT LSCs **(Fig. 4I)**. Proliferation of both $CD8^+$ TCM **(Fig. 4j)** and TEM **(Fig. 4i)** cells was significantly elevated in LSC^{WT} co-cultures, whilst $B2M^{-/-}CIITA^{-/-}$ and $B2M^{-/-}CIITA^{-/-}$CD47OE co-cultures exhibited proliferation levels comparable to baseline.

In ALI co-cultures, proliferating pan T cells followed a pattern consistent with that observed in LSC co-cultures, with significantly higher proliferation detected in co-cultures with WT ALI-derived cells compared to $B2M^{-/-}CIITA^{-/-}$ and $B2M^{-/-}CIITA^{-/-}$CD47OE ALI clones **(Fig. 5b)**. Similarly, no significant differences in $CD4^+$ helper T cell proportions were observed between any of the ALI co-culture conditions **(Fig. 5C)**. The pattern of $CD4^+CD25^+$ activated T cell proportions mirrored that seen in LSC co-cultures **(Fig. 5D)**; however, proliferation of activated $CD4^+$ cells differed between conditions when comparing ALI and LSC co-cultures. Proliferation was higher in WT ALI co-cultures (35%) **(Fig. 5d)** compared to WT LSC co-cultures (24.4%) **(Fig. 4d)**, whilst the opposite was observed for $B2M^{-/-}CIITA^{-/-}$ cells, where ALI co-cultures exhibited notably lower proliferation (5.5%) compared to their LSC counterparts (12.4%). In contrast to LSC co-cultures **(Fig. 4d)**, proliferation of activated $CD4^+CD25^+$ cells in $B2M^{-/-}CIITA^{-/-}$ did not differ from $B2M^{-/-}CIITA^{-/-}$CD47OE ALI co-cultures or from baseline **(Fig. 5d)**. $CD4^+$ TEM proportions and proliferation in ALI co-cultures **(Fig. 5E, e)** were comparable to those observed in LSC co-cultures. In contrast, $CD4^+$ TCM proliferation differed between ALI and LSC conditions: WT ALI co-cultures **(Fig. 5f)** showed markedly higher TCM

proliferation than WT LSC **(Fig. 4f)** co-cultures (53.5% vs 39.1%), whereas the opposite trend was observed for $B2M^{-/-}CIITA^{-/-}$ cells, in which ALI co-cultures exhibited substantially lower proliferation than their LSC counterparts (8.3% vs 21.7%). Unlike in LSC co-cultures, $CD4^+$ TCM proliferation in $B2M^{-/-}CIITA^{-/-}$ did not differ from $B2M^{-/-}CIITA^{-/-}$CD47OE ALI co-cultures or from baseline **(Fig. 5f),** both remaining significantly lower than the WT group.

$CD8^+$ cytotoxic T cell proportions in ALI co-cultures **(Fig. 5G)** were comparable to those observed in LSC co-cultures **(Fig. 4G)**. However, unlike in LSC co-cultures, $CD8^+$ T cell proliferation in WT ALI co-cultures (15.6%) was markedly lower than in WT LSC co-cultures (30.7%) and comparable to both $B2M^{-/-}CIITA^{-/-}$ and $B2M^{-/-}CIITA^{-/-}$CD47OE ALI co-cultures **(Fig. 5g)**. The proportion of activated $CD8^+CD25^+$ cells was higher in WT ALI co-cultures (22%) relative to $B2M^{-/-}CIITA^{-/-}$ (8.6%) and $B2M^{-/-}CIITA^{-/-}$CD47OE ALI clones (8.47%-10.3%) **(Fig. 5H)** yet remained significantly lower than that observed in WT LSC co-cultures (43.5%) **(Fig. 4H)**. Similarly, proliferation of activated $CD8^+CD25^+$ cells in WT ALI co-cultures (3%) was substantially lower than in WT LSC co-cultures (18%), though still significantly higher than in $B2M^{-/-}CIITA^{-/-}$ and $B2M^{-/-}CIITA^{-/-}$CD47OE ALI co-cultures **(Fig. 5h)**.

No significant differences in $CD8^+$ TEM or TCM proportions or their proliferation were observed between any ALI co-culture conditions **(Fig. 5I, J)**. However, when comparing WT ALI to WT LSC co-cultures, a consistent reduction was evident across TEM proportion (20.2% vs 30.9%) **(Fig. 5I)**, TEM proliferation (23.5% vs 53.6%) **(Fig. 5i)**, and TCM

proliferation (13.1% vs 30.5%) **(Fig. 5j)**, collectively indicating an attenuated $CD8^+$ memory T cell response in ALI-differentiated cells.

Together, these findings demonstrate a clear hierarchy of immunogenicity among the generated LSC lines. WT LSCs triggered an alloresponse characterised by significant proliferation across pan, $CD8^+$, $CD4^+$, and memory T cell compartments, alongside robust activation of both $CD4^+$ and $CD8^+$ T cells, consistent with direct and indirect allorecognition. $B2M^{-/-}CIITA^{-/-}$ LSCs provoked a reduced response, predominantly reflected in $CD4^+$ T cell activation and memory proliferation, suggestive of indirect allorecognition mediated by the APCs present in the $CD3^-$ PBMC compartment. In contrast, $B2M^{-/-}CIITA^{-/-}$CD47OE LSCs evaded the immunorecognition, with T cell activation and proliferation across all subsets remaining similar to the baseline. ALI-differentiated derivatives broadly recapitulated this immunogenic hierarchy; however, especially in the cytotoxic CD8+ T cell compartment, the alloresponse was globally attenuated compared to LSCs. Although WT ALI cells retained the capacity to induce higher $CD4^+CD25^+$ proportions and proliferation than their HLA-ablated counterparts and CD47-overexpressing ALI clones, the latter two were largely indistinguishable from baseline, suggesting that, unlike in LSC co-cultures, ALI differentiation in $B2M^{-/-}CIITA^{-/-}$ cells confers additional protection against APC-mediated indirect allorecognition.

Overexpression of CD47 protects LSC $B2M^{-/-}CIITA^{-/-}$ cells from macrophage phagocytosis

549 Given that $CD4^+$ T cell activation in HLA-I/II-ablated LSC co-cultures implicates APC-
550 mediated indirect allorecognition, we next investigated whether CD47 overexpression
551 protects LSCs and their ALI derivatives from macrophage phagocytosis. To examine
552 macrophage phagocytic activity, target cells were labelled with pHrodo Red, a pH-
553 sensitive fluorescent dye that emits signal upon phagocytic engulfment. Labelled target
554 cells (LSC / ALI differentiated - WT, $B2M^{-/-}CIITA^{-/-}$ & $B2M^{-/-}CIITA^{-/-}$CD47OE clones) were
555 subsequently treated with or without an anti-CD47 blocking antibody prior to addition
556 onto macrophage-seeded wells at an Effector: Target (E: T) ratio of 1.2:1 (**Fig. S7B**).
557
558 Macrophage phagocytosis was monitored by live cell imaging every 30 minutes over a 6-
559 hour period across four donors for LSCs and three donors for ALI differentiated cells.
560 Representative fluorescence images at the 3.5-hour timepoint shown in **Figure 6E** and **J**.
561 Anti-CD47 antibody blocking treatment significantly increased macrophage
562 phagocytosis of both LSC **(Fig. 6A, D)** and ALI **(Fig. 6F, I)** target cells across all lines,
563 including WT and the generated clones. In untreated LSC conditions, $B2M^{-/-}CIITA^{-/-}$
564 CD47OE clones displayed macrophage engulfment comparable to that of WT LSCs,
565 whilst $B2M^{-/-}CIITA^{-/-}$ LSCs exhibited greater phagocytic uptake relative to both WT and
566 $B2M^{-/-}CIITA^{-/-}$CD47OE clones **(Fig. 6B, D)**. Following anti-CD47 antibody blockade, the
567 phagocytic index increased in all of the conditions (**Fig. 6D**) with $B2M^{-/-}CIITA^{-/-}$ LSCs
568 exhibiting the highest phagocytic activity, while CD47-overexpressing clones displayed
569 engulfment levels comparable to WT **(Fig. 6C)**.
570
571 Overall, the phagocytic uptake was lower in ALI differentiated cells compared to their LSC
572 counterparts. ALI $B2M^{-/-}CIITA^{-/-}$ cells recapitulated the pattern observed in LSCs,

exhibiting higher phagocytic activity relative to both WT and CD47-overexpressing clones **(Fig. 6G, I)**. Following anti-CD47 blockage, B2M$^{-/-}$CIITA$^{-/-}$ exhibited the highest phagocytic ability relative to WT and B2M$^{-/-}$CIITA$^{-/-}$CD47OE LSCs **(Fig. 6H, I)**.

Taken together, these results demonstrate that LSCs exhibit a greater susceptibility to macrophage phagocytosis than their ALI-differentiated counterparts. Nonetheless in both cell types, CD47 overexpression reduced phagocytic uptake to levels comparable to HLA-I-expressing WT LSCs, suggesting that CD47 can compensate for the loss of HLA-I-mediated "don't eat me" signalling.

LSC B2M$^{-/-}$CIITA$^{-/-}$ and LSC B2M$^{-/-}$CIITA$^{-/-}$C47OE clones are resistant to NK cell cytotoxicity

To investigate whether the CD47 overexpression in LSC B2M$^{-/-}$ CIITA$^{-/-}$ cells inhibits the NK cell-mediated killing response triggered by HLA class I deficiency, we performed coculture experiments. Primary allogenic NK cells were isolated (**Fig. S7C**) from PBMCs using negative MACS separation and were stimulated with IL-2 for 48 hours before and during coculture. K562 cells, naturally lacking HLA class I and II and highly sensitive to NK cell activity, were used as a positive control (**Fig. 7A**). LSC WT, LSC B2M$^{-/-}$CIITA$^{-/-}$ and LSC B2M$^{-/-}$CIITA$^{-/-}$C47OE clones were cocultured with allogenic NK cells at Effector: Target (E: T) ratios of 1:1 (n=5) and 2:1 (n=3) for 56 and 48 hours respectively (**Fig. 7B, C**).

Target cells were grown on xCELLigence RTCA E-Plates for real-time monitoring of NK cell cytolytic activity. A drop of the cell index indicates target cell death, as shown in the 2% Triton-X (Tx2%) lysis control (**Fig. 7C**). As expected, increasing NK cell ratios result in enhanced cytotoxicity against K562 cells (**Fig. 7A**), whereas WT LSCs were completely protected from NK cell-mediated killing at both 1:1(**Fig. 7B**) and 2:1(**Fig. 7C**) E:T ratios. To our surprise $B2M^{-/-}CIITA^{-/-}$ LSCs also evaded NK cell-mediated killing despite the complete absence of HLA-I. Consistent with these findings, both clones overexpressing CD47 similarly evaded NK cell cytotoxicity, indicating that CD47 overexpression does not confer additional protection against NK cell-mediated lysis in HLA-I and HLA-II deficient LSCs (**Fig. 7B, C**).

Surface expression of the degranulation marker CD107a was analysed by flow cytometry as a readout of NK cell activation in response to both LSC-generated cells and corresponding ALI-differentiated derivatives (**Fig. 7D**). NK cells cultured alone were used to establish baseline degranulation, while NK cells co-cultured with K562 cells served as a positive control. Across the three NK donors used for LSC co-culture, baseline degranulation averaged 6.11%. Upon co-culture with K562 cells, CD107a expression increased significantly to 41%. NK cell degranulation remained significantly lower across all LSC variants compared to the K562 positive control. Specifically, CD107a expression was 2.31% for WT LSC and ranged from 3.9% to 7.95% for the LSC $B2M^{-/-}CIITA^{-/-}$ and $B2M^{-/-}CIITA^{-/-}$C47OE clones, all of which represent a marked contrast to the high degranulation triggered by K562 cells (**Fig. 7D**). Furthermore, degranulation across these groups did not differ significantly from the baseline observed in NK-only cultures. A notable exception

was LSC WT, which exhibited significantly fewer CD107a-positive cells (2.31%) than the LSC B2M$^{-/-}$CIITA$^{-/-}$C47OE clone 35 (7.95%).

For the three NK cell donors evaluated in co-culture with ALI-differentiated cells, baseline CD107a expression was 4.54%, which increased significantly to 37.96% upon co-culture with K562 cells (**Fig. 7D**). In contrast, degranulation levels remained at baseline levels when NK cells were co-cultured with ALI-differentiated cultures, including WT (4.06%), B2M$^{-/-}$CIITA$^{-/-}$ (3.9%), and the B2M$^{-/-}$CIITA$^{-/-}$C47OE clones 17 and 35 (2.68% & 2.67%). No significant differences were observed between these groups and the baseline.

To test whether NK cell resistance in HLA-I-ablated B2M$^{-/-}$CIITA$^{-/-}$ LSCs was attributable to physiologically elevated CD47 and/or PD-L1 expression, we pretreated WT and B2M$^{-/-}$CIITA$^{-/-}$ LSCs with anti-CD47 and/or anti-PD-L1 blocking antibodies before and during co-culture. To minimise antibody-dependent cellular cytotoxicity (ADCC), we blocked NK cell Fc receptors 4 hours before co-culture initiation. Real-time xCELLigence monitoring revealed that B2M$^{-/-}$CIITA$^{-/-}$ LSCs evaded NK cell-mediated killing across all blocking conditions, with impedance profiles similar to the target-only control. This was further corroborated by NK cell degranulation and granzyme B release, neither of which differed significantly from WT LSC co-cultures or baseline levels in contrast to the response elicited by the K562 positive control.

Collectively, these findings indicate that the NK cell resistance exhibited by $B2M^{-/-}CIITA^{-/-}$ LSCs is independent of CD47 and PD-L1 signalling, suggesting that alternative mechanisms may underlie their evasion of missing-self cytotoxicity.

Discussion

Hypoimmune engineering of human LSCs represents a promising strategy to establish a universal, well-characterised allogeneic cell source for the treatment of both unilateral and bilateral LSCD, circumventing the need for systemic immunosuppression in recipients, reducing donor variability, and avoiding rejection. To achieve this, LSCs need to be genetically engineered to evade recognition by both innate and adaptive immune responses. However, the development of a clinically relevant, clonally selected cell bank capable of serving a broad patient population necessitates prolonged *in vitro* expansion while preserving stem cell identity and function. In this context, inhibition of the ROCK pathway, commonly employed in stem cell culture, has been shown to support long-term maintenance and expansion of human limbal epithelial stem cells *in vitro* [53]. Moreover, ROCK inhibitors have demonstrated clinical utility in promoting corneal epithelial regeneration and resolving partial LSCD [54].

In this study, we demonstrate that LSCs can be maintained in culture for over 35 passages in the presence of the Ri Y-27632, while preserving their transcriptomic identity and maintaining characteristic limbal stem/progenitor features. Specifically, Ri-treated cultures retained characteristic cobblestone epithelial morphology, sustained

proliferative capacity, maintained their CFE and stable expression of key stem cell markers, including p63 and KRT15. Furthermore, wound healing capacity was enhanced in Ri-treated cultures. Transcriptomic analysis comparing LSCs and ALI-differentiated cells across passages demonstrated that Ri-treated LSCs retained sustained expression of limbal stem/progenitor markers, accompanied by low levels of differentiation-associated genes. In contrast, untreated LSC cultures exhibited a progressive decline in stem cell marker expression, alongside an increase in differentiation markers over time. ALI-differentiated cultures from both Ri-treated and untreated conditions exhibited comparable transcriptional signatures, indicating that ROCK inhibition did not impair differentiation potential across passages.

Interestingly, early-passage LSC cultures exhibited relatively high expression of differentiation markers, including *KRT3, KRT12*, and the suprabasal corneal marker *HES1*. This likely reflects the heterogeneous nature of the initial cell population following enzymatic digestion of human limbal tissue, which may include limbal stem/progenitor cells and more differentiated epithelial cells from the peripheral cornea. Over subsequent passages, a progressive reduction in these differentiation markers was observed. In Ri-treated cultures, this shift was more pronounced, suggesting a selective loss of post-mitotic keratinocytes and enrichment of the LSC population over time. This interpretation is supported by the U-shaped curve of CFE in R+ cultures, and the progressive enrichment of *p63* expression in Ri-treated LSCs across passages. Although Ri-treated LSCs remain transcriptionally comparable to early-passage cells, retain equivalent *in vitro* differentiation potential and stratify under ALI conditions, exhibiting polarity like the native epithelium, further functional validation is required. In particular,

transplantation studies in LSCD animal models comparing early- and late-passage Ri-treated cells for their ability to restore the corneal epithelium, would be essential to confirm their regenerative capacity *in vivo*.

From a translational perspective, the integration of ROCK inhibitor Y-27632 into a GMP-compliant manufacturing workflow is an important consideration for the clinical applicability of this approach. Y-27632 is commercially available as a GMP-grade reagent and has already been incorporated into several clinical-grade stem cell culture protocols, supporting its compatibility with regulatory manufacturing standards [55-57] . Although this would require careful validation of downstream product safety. In addition, for a hypoimmune LSC bank to be clinically scalable, batch-to-batch consistency, cryopreservation resilience, and post-thaw functional stability will be essential parameters to define. With respect to scalability, the prolonged expansion capacity conferred by Ri treatment is particularly advantageous, as it supports the generation of large cell numbers from a limited donor source. However, extensive passaging inherently raises concerns regarding genomic stability, and for clinical applications it is necessary to screen for a genetically stable donor-derived LSC line.

After confirming that LSCs maintained their identity in long-term cultures with R+ we simultaneously delivered Cas9 RNPs containing sgRNAs targeting both *B2M* and *CIITA* loci. We specifically deleted HLA-I, to protect the target cells from CD8+ cytotoxic T cell recognition and HLA-II to protect them from CD4+ helper recognition. Additionally, we overexpressed CD47 to inhibit the innate immune system activation triggered by HLA-I deficiency. Allogeneic T cell co-culture assays revealed distinct modes of immune

recognition across the generated LSC lines. WT LSCs elicited robust activation and proliferation of both $CD4^+$ and $CD8^+$ T cells, consistent with classical direct allorecognition mediated by donor HLA class I and II molecules. In contrast, $B2M^{-/-}CIITA^{-/-}$ LSCs, lacking surface HLA, avoided direct recognition but induced a response dominated by $CD4^+$ T cell activation and proliferation, with limited $CD8^+$ activation but no proliferation. This profile is consistent with indirect allorecognition, whereby phagocytic uptake by antigen-presenting cells enables presentation of processed alloantigens to $CD4^+$ T cells, with delayed, helper-dependent $CD8^+$ response.

Enhanced susceptibility of $B2M^{-/-}CIITA^{-/-}$ LSCs to macrophage phagocytosis supports this mechanism, reflecting loss of HLA class I-mediated inhibitory signalling. Increased phagocytic uptake would augment antigen availability and drive indirect alloresponses. CD47 overexpression effectively mitigated this vulnerability, suppressing phagocytosis via SIRPα engagement and limiting antigen transfer to APCs. Accordingly, $B2M^{-/-}CIITA^{-/-}$CD47OE LSCs exhibited complete immune evasion, with T cell responses reduced to baseline and macrophage phagocytic activity equal to that of WT. In ALI-differentiated cultures, this hierarchy was preserved but attenuated. Notably, $B2M^{-/-}CIITA^{-/-}$ ALI cells failed to elicit detectable $CD4^+$ responses, consistent with reduced phagocytic susceptibility, thus limiting antigen availability for indirect presentation via host APC HLA-II. $CD8^+$ responses were also globally diminished, particularly in WT conditions. This attenuation likely reflects both reduced antigen transfer and differentiation-associated immunomodulation, including increased PD-L1 expression, which may suppress cytotoxic T cell activity via PD-1 engagement.

Surprisingly, dual knockout of *B2M* and *CIITA* in LSCs did not elicit a "missing self" NK cell-mediated cytotoxic response, nor did CD47 overexpression confer additional protection. Missing-self theory predicts that HLA class I loss should sensitise a target to NK-mediated lysis by removing inhibitory KIR and NKG2A ligands [38,39], and this prediction has held in numerous other HLA-ablated cell systems, where $B2M^{-/-}$ products have repeatedly been shown to be susceptible to NK killing [299]. Vulnerability that has, in fact, been the central rationale for pairing HLA ablation with CD47 overexpression [26], HLA-E [58] or HLA-G [59,60] knock-in, or other inhibitory ligands in hypoimmune engineering. $B2M^{-/-}CIITA^{-/-}$ LSCs did not follow this pattern. They were fully resistant to NK-mediated killing, indistinguishable from WT and from the CD47-overexpressing clones across both E:T ratios. We initially hypothesised that this could be attributed to the intrinsically high expression of CD47 and PD-L1 in LSCs; however, blockade of endogenous CD47 and PD-L1 in $B2M^{-/-}CIITA^{-/-}$ LSCs still failed to induce an NK cell response. This rules out the two most obvious candidate checkpoints and indicates two potential explanations equally important and non-mutually exclusive. The missing self-recognition is either not effectively engaged in $B2M^{-/-}CIITA^{-/-}$ LSCs due to other inhibitory axes not tested here or there is that primary LSCs simply present a low baseline density of NK-activating ligands, keeping the net activating signal below the threshold required for lysis regardless of HLA-I inhibitory ligand loss. Both scenarios are consistent with the general principle that HLA-I loss alone is necessary but not sufficient to trigger NK killing [61].

Together, these data define a dual-layered strategy for immune evasion: genetic ablation of HLA class I and II combined with CD47 overexpression suppresses both direct and

indirect allorecognition, while epithelial differentiation further reinforces immune privilege through reduced phagocytosis and checkpoint-mediated inhibition. Whether hypoimmune engineering or prolonged *ex vivo* expansion alters the capacity of LSCs to integrate into and respond to limbal niche signals remains an important open question. *In vivo* transplantation studies in LSCD animal models will be essential to determine whether engineered cells can reconstitute a functional, self-renewing corneal epithelium rather than merely engraft transiently.

However, it is important to acknowledge that HLA class I and II molecules, whilst the predominant drivers of allorecognition, do not represent the complete landscape of transplant rejection antigens. Corneal epithelial cells express ABO blood group antigens[62,63], and in the event of donor-recipient ABO incompatibility, graft-expressed antigens may become targets of pre-existing recipient AB antibodies, leading to antibody-dependent cellular cytotoxicity (ADCC) and complement-dependent toxicity (CDC) [64]. Additionally, the H-Y antigen system, encoded by Y chromosome-linked genes constitutes a clinically relevant barrier in male-to-female transplantation, where recipient immune responses against H-Y peptides have been associated with graft rejection [65]. Hence, to minimise residual allorecognition and rejection, careful donor selection should therefore complement the hypoimmune engineering strategy: specifically, the use of LSCs derived from donors of blood group O and XX genotype individuals. However, given the residual uncertainty regarding the extent to which ABO antigens contribute to corneal immune recognition *in vivo,* donor selection based on blood group O may be viewed as a conservative strategy to reduce potential antibody-mediated risk rather than a definitive requirement.

The corneal epithelium serves as a critical barrier continuously exposed to environmental insults and pathogens. Although the depletion of HLA class I and II molecules warrants further investigation in this context, the ocular surface is supported by a multilayered innate defence system, including the antimicrobial and immunomodulatory properties of the tear film, as well as resident immune cell populations within the limbal niche and central cornea, which may partially compensate for reduced antigen-presenting capacity in HLA-ablated limbal/corneal epithelial cells [66], remains an important question for future preclinical studies.

Beyond immunological rejection, the immune-evasive properties of hypoimmune LSCs introduce distinct biosafety considerations that must be carefully weighed against their therapeutic promise. The very mechanisms that protect transplanted cells from immune clearance could, in a malignant or genomically unstable state, impair immunosurveillance and thereby increase the risk of unchecked persistence, expansion or migration. One potential mitigation strategy is the incorporation of inducible suicide switches into the engineering cassette, enabling selective ablation of transplanted cells should adverse events arise. An additional concern, which warrants evaluation, is the potential transfer of CD47-enriched extracellular vesicles to bystander tissues, where they could theoretically confer a transient “don’t eat me” signal to otherwise immunologically normal cells.

These risks must, however, be considered in the context of the substantial burden imposed by current standard-of-care therapy. Conventional allogeneic LSC

transplantation requires long-term systemic immunosuppression, with well-recognised risks of opportunistic infection, secondary malignancy, and reduced quality of life, and is also limited by poor long-term graft survival due to rejection. In contrast, a successful hypoimmune allogeneic therapy could eliminate this pharmacological burden while supporting durable engraftment. By comparison, autologous therapies have a stronger track record of long-term survival; however, 1/3 of grafts still fail for reasons unrelated to rejection, including donor-related variability and niche damage. A well-characterised and easily available LSC product could help overcome this source of variability. At the healthcare system level, an off-the-shelf product derived from a single engineered cell line would also reduce the logistical and financial costs associated with autologous cell harvesting, donor matching, and post-transplant immunosuppression monitoring. Ultimately, advancement of hypoimmune LSC platforms should rest on a transparent risk-benefit framework that acknowledges biosafety uncertainties while recognising the therapeutic advantages of immune-tolerant allogeneic therapies.

Materials and Methods

Human tissue donation

Adult human eyes from three donors were donated for research following informed consent. All tissue was provided by NHS Blood and Transplant Tissue and Eye Services or the Newcastle NHS Trust following ethical approval (18/YH/04/20). Whole eyes were

delivered covered in PBS and processed within 24h after enucleation. Details of the three donors are provided in **Table S1**.

LSC cell isolation and *ex vivo* expansion

Preparation of 3T3-J2 feeder cells

Twenty-four hours before seeding LSCs, 3T3-J2 mouse fibroblasts (Cat. EF3003, Karafast, USA) were mitotically inactivated using Faxitron x-ray, with a current of 4mA, and a voltage of 120kv for 7 minutes. Mitotically inactivated 3T3-J2 cells were suspended in feeder cell media containing high-glucose DMEM (Cat. 31966-02, Gibco) supplemented with bovine calf serum (10%) (HyClone Cat. SH30072.03, USA) and penicillin/streptomycin (1%) (Gibco, Cat. 15140122) and plated at the final density of 4 $\times 10^4$ cells per cm^2 in 9.6 cm^2 tissue culture dishes. The cells were incubated on a humidified tissue culture incubator overnight at 37°C, containing 5% CO_2 to allow the establishment of a feeder layer.

LSCs isolation from eye tissue using enzymatic digestion

LSCs were harvested from cadaveric donor cornea-scleral rims (CSR) using serial enzymatic digestion of the tissue. Briefly described, the CSR was isolated from the whole eye, and the excessive tissue was dissected, leaving a ring containing approximately 2 mm of peripheral cornea and 2 mm of adjacent sclera. The remaining ring containing the limbus was further chopped in $1mm^2$ pieces. LSCs were isolated from these pieces using

0.5% trypsin-EDTA (Gibco, Cat. 25300062) solution for 20 minutes at 37°C. After the incubation, the supernatant containing the resulting dissociated LSCs was collected and FBS containing epithelial media was added to neutralise the trypsin. The LSCs were pelleted by spinning at 1000rpm for 5 minutes. After removing the supernatant, the cells were re-suspended in epithelial medium containing, 65% Low Glucose Dulbecco's Modified Eagle Medium (DMEM) (Cat. 21885-025, Gibco), 25% Ham's F12 medium (Cat. 31765-027, Gibco), FBS 10% (Cat.10270-106, Gibco), hydrocortisone 0.4 µg/ml (Cat. H2270, Sigma Aldrich), insulin 5 µg/ml (Cat. I9278, Sigma Aldrich), triiodothyronine 1.4 ng/ml (Cat. T5516, Sigma Aldrich), adenine 24 µg/ml (Cat. A9795, Sigma Aldrich), cholera toxin 8.4 ng/ml (Cat. C8052, Sigma Aldrich), EGF 10 ng/ml (Cat. E9644 Sigma Aldrich) and 1% of penicillin/streptomycin (Gibco, Cat. 15140122). This procedure was repeated three more times using the same limbal tissue. The isolated cells were pooled together, and 30,000 viable LSCs (density of $3.125 \times 10^3/cm^2$) in epithelium media were added to a 9.6 cm^2 tissue culture well coated with 3T3-J2 feeder cells.

Serial LSC expansion on 3T3-J2 feeder layer

Human limbal epithelial stem cell expansion on mitotically inactivated J2-3T3 feeder cells was performed using the described above epithelial media. The epithelial medium was supplemented with 10 µM ROCK inhibitor (Ri, Y27632, Tocris) when indicated. Cell colonies with typical epithelial morphology started to appear after 2–5 days and were cultured until they became subconfluent. Following this, the remaining 3T3-J2 feeder cells were detached and removed from the coculture using 1x Versene (Gibco, Cat. 15040066), and subconfluent LSCs were dissociated with 0.5% trypsin-EDTA (Gibco, Cat.

25300062) to single-cell suspension and plated at a density of 3.125 × 10^3 cells/cm2 onto fresh wells preplated with mitotically inactivated J2-3T3 feeder cells.

Colony forming efficiency (CFE)

500 LSCs were seeded with or without Ri, in feeder coated 6 well plates. After 8-12 days in culture, the cells were fixed in 4% PFA and stained with 2% Rhodamine B (in H_2O). The colonies were counted, and the CFE was calculated using the following equation:

$$CFE = \left(\frac{Colonies\ counted}{500}\right) x100$$

Air-Liquid Interface (ALI) Differentiation of LSCs

For ALI differentiation, 2.5×10^5 LSCs were seeded onto feeder-coated 24-well ThinCert® Cell Culture Inserts (Greiner Bio-One), with feeder cells present both on the insert membrane and in the basal compartment. Cells were maintained in epithelial medium with or without 10 μM Y-27632 (Ri), with 500 μL added to the basal compartment and 250 μL to the apical compartment. Cells were allowed to adhere overnight, after which the medium was transitioned to a 1:1 mixture of epithelial and differentiation medium (65% low-glucose DMEM (Cat. 21885-025, Gibco), 25% Ham's F-12 (Cat. 31765-027, Gibco), 10% FBS (Cat. 10270-106, Gibco), hydrocortisone 0.4 μg/mL (Cat. H2270, Sigma-Aldrich), insulin 5 μg/mL (Cat. I9278, Sigma-Aldrich), triiodothyronine 1.4 ng/mL (Cat. T5516, Sigma-Aldrich), cholera toxin 8.4 ng/ml (Cat. C8052, Sigma Aldrich), adenine 24 μg/mL (Cat. A9795, Sigma-Aldrich), KGF 10 ng/mL (Cat. 100-19-50UG, PeproTech®),

and 1% penicillin-streptomycin (Cat. 15140122, Gibco)), with or without Ri, applied to both compartments. The following day, the medium was replaced entirely with differentiation medium and replenished every other day. At the end of week 1, the apical medium was removed to establish the ALI, and cells were maintained for a further two weeks. To promote epidermal stratification, partial basal feeding was performed daily throughout the ALI phase.

Wound healing assay

LSCs from three independent donors were seeded at 50,000 cells/well in 96-well ImageLock® plates (Sartorius, Cat. No. BA-04856) and incubated for 6 hours at 37°C in a humidified 5% CO_2 incubator to establish a confluent monolayer. Uniform scratch wounds were introduced simultaneously across all wells using the IncuCyte® WoundMaker tool (Sartorius) according to the manufacturer's instructions. Wells were subsequently washed twice with PBS to remove cellular debris. Immediately after wounding, cells were treated with the Rho kinase inhibitor Y-27632 (Ri; 10 μM) or left untreated. Plates were transferred to the IncuCyte® S3 Live-Cell Analysis System (Sartorius) housed within a humidified incubator (37°C, 5% CO_2), and phase-contrast images were acquired automatically at 3-hour intervals over 48 hours using a 10× objective. Wound closure dynamics were quantified using the IncuCyte® Scratch Wound Cell Migration Software Module. The wound confluence (%) and relative wound density (RWD, %), defined as the density of cells in the wound area relative to the density outside the wound area, were calculated over time.

DNA extraction and PCR

Genomic DNA (gDNA) was extracted using QIAamp DNA Mini Kit (Cat. 56304, Qiagen) and quantified with NanoDrop™ 2000/2000c Spectrophotometers (Thermo Scientific™). 1.25U of GoTaq® G2 DNA Polymerase (Cat. M7841, Promega) was used in a 50ul PCR reaction, composed of 10ul GoTaq® Reaction Buffer(5X) (Cat. M7921, Promega), 1ul of PCR Nucleotide Mix (final concentration 0.2mM) (Cat. U1511, Promega), 1ul of each 10mM, F and R primer, 2ul of gDNA and Nuclease-Free Water to 50ul. The primer sequences are shown in **Table S4.**

RT-qPCR

ReliaPrep™ RNA Cell Miniprep Kit was used to extract RNA from cell pellets following manufacturer's instructions. RNA quantification was performed with Qubit™ RNA Broad Range (BR). RNA to cDNA conversion was performed using Promega GoScript™ Reverse Transcription Kit with 200ng of RNA input. Experiments were conducted using a QuantStudio™ 7 Flex Real-Time PCR machine (Applied Biosystems, UK), using SYBR green reaction technology (Promega, UK). The cDNA was amplified by heating to 95 °C for 10 minutes followed by 40 cycles of 95 °C for 15 seconds and 60 °C for 1 minute (using ramp rate of 1.6 °C s−1), with a final heating step of 95 °C for 15 seconds. *GAPDH* was used as housekeeping gene, and when indicated, cornea from donor tissue or early passage LSCs were used as controls. The relative gene expression was assessed using the primers in **Table S5.**

Bulk RNA-Seq

Following cell isolation from limbal tissue LSCs were cultured with (+) or without (-) Ri. Throughout the passages LSCs or ALI derived cultures were collected, and RNA was extracted from the samples using ReliaPrep™ RNA Cell Miniprep Kit. Samples were processed for sequencing using the Illumina Stranded mRNA Library Prep Kit (Illumina) following manufacturer's instructions. Libraries were sequenced (101 bp paired end reads) on an Illumina NovaSeq 6000. Reads were quality checked using FastQC and MultiQC. Reads were quantified by Salmon software (version 1.9.0) using the Human (GRCh38) transcriptome from Gencode (release version 42). The resulting count tables were imported into R (version 4.2.2) with tximport (version 1.26.1), and normalization and differential expression analysis was carried out with DESeq2 (version 1.38.2). Data are publicly available through the NCBI Gene Expression Omnibus (GEO) under accession number: GSE329486. Significant DEGs were identified by absolute value of log2(FoldChange) >= log (2) = 1 & adjusted p-value <= 0.05.

Immunofluorescence analyses

Membranes of hanging inserts where the differentiated limbal epithelial cells adhered, were cut, and fixed with 4% paraformaldehyde (PFA) at RT for 20 min. The cells were blocked and permeabilised using 10% donkey serum + 0,3% Triton X100 in PBS solution. Differentiated limbal epithelial cells were incubated with primary antibodies (**Table S7**)

overnight at 4°C and for 1 hour at room temperature with the secondary antibody. Following each antibody incubation, samples were washed three times for 10 minutes each. Images were acquired as z-stacs with an Axio Imager 4 with Apotome structured illumination fluorescence. Maximum intensity projections were generated in ZEN software, with image brightness and contrast uniformly adjusted based on a secondary antibody control.

Enrichment of cultured LSCs (Collagen IV quick adhesion assay)

To enrich LSCs and eliminate the residual feeder cells, 6 well culture dishes, were coated with human collagen IV (20 µg/mL) for 2 hours at room temperature (RT) and then incubated with 0.5 mg mL−1 heat-denatured BSA in PBS at 37°C for 1 hour and rinsed with medium before use. The cell suspension (containing 3T3s and LSCs) was allowed to attach to col-IV for 30 minutes at 37 °C. The wells were washed twice delicately with PBS to eliminate the residual 3T3s. The attached LSCs were then lifted using 0.5% trypsin-EDTA (Gibco, Cat. 25300062).

Flow cytometry in LSCs

Enriched LSCs or ALI differentiated derivatives were first incubated on ice with human Fc receptor (FcR) Blocking Reagent (Cat. 130-059-901, Miltenyi Biotec) for 5 minutes to prevent non-specific antibody binding. Following blocking, cells were stained with fluorochrome-conjugated antibodies or their respective isotype controls for 30 minutes

at 4 °C **(Table S8)**. After staining, cells were washed three times with FACS buffer (2% FBS in PBS), resuspended in 500 µL of FACS buffer, and kept on ice until analysis.

For intracellular staining, cells were fixed and permeabilised by the gradual addition of 70% chilled ethanol to the cell pellet while vortexing for 30 seconds. The samples were then incubated at -20 °C for 1 hour. After fixation, cells were washed twice with FACS buffer and resuspended in 100 µL of appropriately diluted fluorochrome-conjugated antibodies for 30 minutes at room temperature (RT). Following three additional washes with FACS buffer, cells were resuspended in 500 µL of buffer. Flow cytometry analysis was performed using a BD LSRFortessa™ Cell Analyser. Data were analysed using FSC express 7 software.

HLA-I and HLA-II ablation in LSCs

Simultaneous ablation of HLA class I and class II surface expression was achieved by co-delivery of *B2M*- and *CIITA*-targeting Cas9 ribonucleoproteins (RNPs) into LSCs via nucleofection. Briefly, 200 pmol of each sgRNA (*B2M* and *CIITA,* (**Table S3**) were individually pre-complexed with 100 pmol of TrueCut™ Cas9 Protein v2 (Thermo Fisher Scientific) for 10 minutes at room temperature to form RNPs prior to pooling. A total of 1 × 10^6 LSCs were resuspended in 100 µL of Human Keratinocyte Nucleofector® Solution (Lonza; Nucleofector® Solution: Supplement ratio of 4.5:1) containing both RNP complexes, transferred to an Amaxa® nucleofection cuvette, and nucleofected using programme T-025. Immediately following nucleofection, 500 µL of epithelial medium supplemented with 10 µM ROCK inhibitor (Y-27632; Tocris) was added, and cells were gently resuspended using a Pasteur pipette. Cells were subsequently plated at a 1:6 ratio

onto feeder-coated 6-well plates and expanded until semi-confluent. The pooled edited population was then treated with 100ng/ml of IFN-γ to upregulate HLA surface expression, detached, and FACS sorted for clonal isolation of HLA-I/HLA-II double-negative cells into individual wells of 96-well plates pre-coated with feeder cells and supplemented with 10 μM Y-27632.

Lentiviral transduction of HLA-I and HLA-II ablated cells

To determine the optimal multiplicity of infection (MOI) for *B2M*$^{-/-}$ *CIITA*$^{-/-}$ LSCs, control lentivirus expressing mCherry reporter under *EF1α* promoter was used to transduce cells across a range of MOIs (0–6) via a centrifugation-based spinfection method in the presence of 5 μg/mL polybrene. Transduction efficiency and median fluorescence intensity (MFI) of mCherry^{+} cells were assessed by flow cytometry 48 hours post-transduction to identify the MOI yielding optimal transgene expression with minimal cytotoxicity.

For stable CD47 overexpression, *B2M*$^{-/-}$ *CIITA*$^{-/-}$ LSCs were transduced with an *EF1α*-human *CD47* lentiviral construct harbouring a blasticidin resistance cassette at the above determined MOI of 4. Briefly, 1 × 10^5 LSCs were resuspended in 100 μL of epithelial medium supplemented with 10 μM Y-27632, 5 μg/mL polybrene, and the CD47 lentiviral vector, and centrifuged at 1,000 × *g* for 1 hour. The supernatant was aspirated, and transduced cells were plated onto blasticidin-resistant 3T3-J2 feeder cells in media supplemented with 10 μM Y-27632 for 72 hours before initiation of antibiotic selection

with blasticidin (6 ug/ml) for one week. Stably transduced cells were subsequently subjected to FACS-based clonal isolation, gating for the highest CD47-expressing population.

Quantification of CD47 Surface Expression

Absolute CD47 molecule counts per cell were quantified using the BD Quantibrite™ PE Quantitation Kit (BD Biosciences) according to the manufacturer's instructions. Briefly, cells were lifted, counted, and washed twice in FACS buffer (PBS supplemented with 2% FBS), after which an equal number of cells per condition were incubated with a PE-conjugated anti-human CD47 antibody (Cat. No. 323108; BioLegend) for 30 minutes at 4°C in the dark. Following two washes, cells were resuspended in FACS buffer and acquired alongside BD Quantibrite™ PE beads on a BD LSRFortessa™ flow cytometer. Quantibrite™ PE beads consist of four discrete populations carrying defined, lot-specific numbers of PE molecules per bead, enabling construction of a standard curve relating PE fluorescence intensity to absolute molecule number. The number of CD47 molecules per cell was interpolated from this standard curve using the mean PE fluorescence intensity of the stained cell population **(Fig. S6D)**. Data were analysed using FSC Express 7 software.

Viral copy number (VCN) quantification via ddPCR

gDNA was extracted using QIAamp DNA Mini Kit (Qiagen) according to the manufacturers recommendations and quantified using Qubit™ dsDNA Quantification Assay. The gDNA

stock was brought to 10ng/ul then diluted at 10-fold dilutions using ultra-pure nuclease-free water, and 5 µl of each dilution was used per reaction in duplicates. VCN was measured by digital droplet PCR (ddPCR) using a FAM-conjugated primer probe targeting the *DelU3* region and a HEX-conjugated primer probe targeting *RPP30*, used as a reference gene. The ddPCR reaction was set up in a 96-well plate format according to the manufacturer's recommendations using the Bio-Rad ddPCR Multiplex Supermix, primers, probes (primer to prob ratio 3.6) **(Table S6)** and gDNA in a final reaction volume of 22 µl. The reaction plate was sealed with adhesive foil seals (Bio-Rad), vortexed vigorously and then shortly spun down. The ddPCR reaction plate was then transferred to the Automated Droplet Generator, and the manufacturer's protocol was followed to generate droplets. The sample droplet plate was then sealed using the recommended foil and sealer and then transferred onto a C1000 Touch thermal cycler (Bio-Rad) where droplets were amplified to endpoint by heating to 95 °C for 10 minutes, followed by 39 cycles of 94 °C for 30 seconds, 60 °C for 1 minute (using ramp rate of 2 °C/s), and 72 °C for 1 minute extension step with a final heating step of 98 °C for 10 minutes. The reacted products were cooled off for 15 minutes at 12 °C before hold. The plate was then placed into the QX200 droplet reader. Using Bio-Rad's QX Manager Software (Standard Edition, version 1.2), the concentration of the target amplicon per microliter for each sample was estimated for both *DelU3* and *RPP30* reference genes. Estimated VCN values were finally calculated by dividing the concentration of the target copies per microliter by the concentration of the reference copies per microliter and multiplied by copy number of reference (VCN = copies DelU3 per µl / copies RPP30 per µl × 1).

Immune coculture assays

Whole blood from healthy adult donors was collected following informed consent **(Table S2)**. Peripheral blood mononuclear cells (PBMCs) were isolated collected by density gradient centrifugation, and immune subsets were further isolated (Pan T cells, Monocytes and NK cells) for immune assays **(Table S2)**. Target and effector cells were HLA-haplotyped, and HLA-A, HLA-B, and HLA-DRB1 loci were assessed for mismatches **(Table S12)**.

PBMC isolation from whole blood

PBMCs were removed from whole blood by density gradient centrifugation on Lymphoprep. The isolation procedure was carried out at RT. Whole blood was diluted 1:1 in HBSS (Ca^{2+}, Mg^{2+} free) supplemented with 2mM EDTA. 25 ml of diluted blood was slowly layered onto 15ml of Lymphoprep and spun at 900g, RT for 30 minutes (Acc 6, brake 6). The buffy coat containing the PBMCs was collected using a sterile Pasteur pipette. The collected PBMCs were transferred into a new tube and washed from Lymphoprep with cold HBSS supplemented with 1% FBS up to 50ml and centrifuged at 600g, 4°C for 8minutes. Two other washes with 300g, 4°C centrifugation for 8 minutes, were performed for removing contaminating platelets.

Pan T cell negative selection by MACS

Pan T cells were negatively selected from PBMCs using magnetic-activated cell sorting (MACS). Briefly, up to 10^7 PBMCs were resuspended in 40 µL of MACS buffer (PBS supplemented with 0.5% BSA and 2 mM EDTA (Cat. E7889, Sigma Aldrich)) and labelled with 10 µL of Pan T Cell Biotin-Antibody Cocktail (Cat. 130-096-535, Miltenyi Biotec) for 5 minutes at 4°C. Following incubation, 30 µL of MACS buffer and 20 µL of Pan T Cell MicroBead Cocktail (Miltenyi Biotec) were added, and the suspension was incubated for a further 10 minutes at 4°C. The magnetically labelled cells were applied onto an LS column (Miltenyi Biotec) placed in a MidiMACS™ Separator, and the flow-through containing unlabelled Pan T cells was collected. The column was subsequently washed with 3 mL of MACS buffer, and the unlabelled fraction was combined with the initial flow-through to maximise T cell yield. The column was then removed from the magnetic field and placed into a suitable collection tube, and the magnetically retained non-T cell fraction was eluted by applying 5 mL of MACS buffer and firmly flushing the plunger into the column; this positive fraction was collected separately as the $CD3^-$ population (CD3+ depleted population). The purity of the negatively selected Pan T cell fraction was assessed by flow cytometry **(Table S2, Table S11, Fig. S7a)**.

Monocyte positive selection by MACS

$CD14^+$ monocytes were positively selected from PBMCs using MACS. Briefly, up to 10^7 PBMCs were resuspended in 80 µL of MACS buffer (PBS supplemented with 0.5% BSA and 2 mM EDTA) and labelled with 20 µL of CD14 MicroBeads Human (Cat. 130-097-052, Miltenyi Biotec) for 15 minutes at 4°C. Following incubation, cells were washed by adding 1 mL of MACS buffer and centrifuged at 300 × *g* for 10 minutes, after which the

supernatant was completely aspirated. The cell pellet was resuspended in 500 µL of MACS buffer and applied onto an LS column (Miltenyi Biotec) placed in a MidiMACS™ Separator. The column was washed three times with 3 mL of MACS buffer, and the flow-through containing unlabelled cells was discarded. The column was then removed from the magnetic field, and magnetically labelled $CD14^+$ cells were eluted by applying 5 mL of MACS buffer and firmly flushing the plunger into the column. The purity of the positively selected $CD14^+$ monocyte fraction was assessed by flow cytometry **(Table S2, Table S11, Fig. S7b)**.

NK negative selection by MACS

NK cells were negatively selected from PBMCs using MACS. Briefly described, using the NK Cell Isolation Kit human (Cat. 130-092-657, Miltenyi Biotec) a maximum amount of 10^7 PBMCs were labelled for 5 minutes at 4°C with the NK Cell Biotin-Antibody Cocktail 1:5 diluted in MACS buffer (PBS, 0.5% BSA and 2mM EDTA) at a final volume of 50 µl. Following the incubation, a total volume of 50 µl of NK Cell MicroBead Cocktail 1:2.5 diluted in MACS buffer was added for 10 minutes at 4°C. The resulting magnetic labelled cells were added onto an LS column (Miltenyi Biotec) placed in a MidiMACS™ Separator. The flow through containing the unlabelled NK cells was collected and the column was further washed with a maximum of 5 ml of MACS buffer to maximise the harvest. The purified NK cells were then analysed by flow cytometry, and only the samples with >80% purity (CD56+ cells) were used for the immune assay applications **(Table S2, Table S11, Fig. S7c)**.

Cell culture of NK cells

Isolated primary NK cells were cultured in RPMI 1640 with 10% heat inactivated FBS and 1% penicillin/streptomycin. NK cells were stimulated with 500 IU human IL-2 (PeproTech) for 48 hours prior and during the assays.

K562 cell culture

K562 cell line was purchased from Merck and cultured in RPMI 1640 with 10% heat inactivated FBS and 1% penicillin/streptomycin.

Macrophage differentiation

$CD14^+$ PBMCs were isolated by MACS as described above. Cells were seeded at 1×10^6 cells/mL in RPMI 1640 supplemented with 10% heat-inactivated FBS and 1% P/S (all Gibco) and incubated overnight in 5% CO2 incubator at 37°C, to allow monocyte adherence. Human M-CSF (Gibco™/PeproTech®, 17852253) was then added at 50 ng/mL. The M-CSF containing medium was replenished every other day until day 6. Differentiated macrophages were detached by incubation with 10 mM EDTA in PBS followed by mechanical scraping, reseeded into 96-well plates at 6×10^5 cells/well, and primed overnight with recombinant human IL-2 (100 IU/mL; PeproTech) before phagocytosis assays.

Allogeneic T Cell Activation and Proliferation Assay

Pan T cells ($CD3^+$) were isolated from PBMCs of four independent allogeneic donors by negative MACS selection as described above, and the corresponding $CD3^-$ PBMC fraction was retained as a source of autologous antigen-presenting cells (APCs). Prior to co-culture, LSC and ALI target cells were seeded and pre-conditioned with IFN-γ (100 ng/mL) for 48 hours. Pan T cells were labelled with CellTrace™ Violet (CTV; 0.2 µM per 1 × 10^6 cells in PBS) for 30 minutes at 37°C in the dark, washed, and resuspended in co-culture medium before use. Co-cultures were established by seeding CTV-labelled Pan T cells (8 × 10^5) together with the $CD3^-$ PBMC fraction (2 × 10^5) onto IFN-γ pre-conditioned target cells in co-culture medium consisting of a 1:1 mixture of complete epithelial medium and X-VIVO™ 15 Media (Lonza) supplemented with 2% human AB serum (MP Biomedicals™ Human Serum, Type AB Cat. 11465055), 1% penicillin-streptomycin, and a final concentration of 20 IU/mL recombinant human IL-2. Partial media changes were performed every three days. To sustain continuous antigen exposure and model a prolonged allogeneic response, co-cultures were maintained for three weeks via weekly serial passage, whereby effector cells were transferred onto freshly seeded, IFN-γ pre-conditioned target cells and $CD3^-$ APCs at each interval. T cell activation and proliferation were assessed by flow cytometry at weekly time points using the following panel: CellTrace™ Violet Cell Proliferation Kit (Cat. C34557); anti-CD4 BUV395 (Cat. 363-0047-42, eBioscience); anti-CD3 BV510 (Cat. 300448, BioLegend); LIVE/DEAD™ Fixable Near-IR viability dye (Cat. L10119; Thermo Fisher Scientific); anti-CD25 PE (Cat. 12-0257-42, eBioscience); anti-CD62L PE/Cy7 (Cat. 304822, Biolegend); anti-CD45RO BV650 (Cat. No. 416-0457-42, eBioscience); anti-CD45 BUV737 (Cat. 367-0459-42, eBioscience); and anti-CD8 APC (Cat. 980904, BioLegend). Unstimulated $CD3^+$ and

CD3⁻ PBMC fractions served as negative baseline controls, while CD3/CD28 Dynabeads™-stimulated T cells were included as a positive control for effector cell activation and proliferation. Flow cytometry analysis was performed using a BD LSRFortessa™ Cell Analyser. Data were analysed using FSC Express 7 software following gating strategy described in **Figure S8**.

Macrophage phagocytosis assay

Macrophage phagocytic activity was assessed using pHrodo™ Red (250 ng/mL; 1 hour, 37°C), a pH-sensitive dye that fluoresces upon internalisation into acidic phagolysosomes. Target cells (LSCs and ALI-differentiated cells) were treated with or without anti-CD47 blocking antibody (10 µg/ml, clone MIAP410, mouse IgG1κ: Cat. BE0283, BioXCell) for 30 minutes prior to and during co-culture; in CD47 blocked conditions, macrophage Fc receptors were pre-blocked for 30 minutes at 37°C. Labelled target cells were seeded onto M-CSF-derived macrophages (generated from $CD14^+$ monocytes as described above) at an E:T ratio of 1.2:1 and imaged using the IncuCyte® Live-Cell Analysis System (10×, phase and orange channels, four images/well, two technical replicates) at 30-minute intervals over 6 hours across four donors (LSCs) and three donors (ALI-differentiated cells). Cytochalasin D (5 µM) and pHrodo™ Red-labelled target cells resuspended in 50 mM acetic acid buffer (pH 4.0) served as negative and positive controls, respectively. Total orange object area (μm^2/image) was quantified per time point and normalised to the maximum positive control fluorescence at T = 0 to yield a normalised phagocytic index, correcting for inter-target variability in cell number and dye incorporation.

NK cell cytotoxicity experiments – XCELLigence

NK cell killing assays were performed on the xCELLigence S16 platform (Agilent Technologies). Specialised 16-well E-plates were coated with collagen-IV (when seeded with LSCs) or CD71 tethering antibody (when seeded with K562s). 5 x 10^4 target cells (LSCs or K562) were plated on the E-plates and attachment, and growth was recorded every 10 minutes for 24 hours. At 24 hours post target cell seeding, IL-2 stimulated effector cells were added at a 1:1 or 1:2 effector to target cell ratio (E: T). 2% Triton-x in media was used as a full lysis control. The cytotoxicity was recorded for a total of 56 hours in 1:1 cultures and 48 hours in 1:2 cultures.

In selected experimental conditions, target cells were pre-treated for 2 hours before co-culture with an anti-human CD47 blocking antibody (10 µg/ml, clone MIAP410, mouse IgG1κ: Cat. BE0283, BioXCell) and/or an anti-PD-L1 blocking antibody (Avelumab, Human IgG1, λ, Cat. SIM0021 BioXCell), which were maintained throughout the duration of the co-culture. To prevent antibody-dependent cytotoxicity, NK cells were pre-incubated with human FcR Block (Cat. No. 130-092-575, 1:5 dilution; Miltenyi Biotec) for 2 hours at 37°C prior to their addition to target cells. Cell index was measured every 2 minutes for the first 6 hours and every 15 minutes for the remaining time. Media used during the coculture was 1:1 epithelial and NK cell media. Data were analysed and normalised using RTCA software PRO 2.9.0 (Agilent Technologies). Supernatants were collected for granzyme B ELISA after 48 hours of co-culture.

Degranulation assay

LSCs and ALI derivatives were cultured at a 1:2 ratio for 6 hours with IL-2 stimulated NK cells. Co culture with K562 cells was used as a positive control for degranulation. After incubation time, NK cells were collected stained with Zombie NIR Fixable Viability Kit (Cat. 423105, Biolegend), anti-CD56-APC (Cat. 981204, Biolegend) and anti-CD107a-PE (Cat. 328608, Biolegend) In selected experimental conditions, target cells were pre-treated for 2 hours before co-culture with an anti-human CD47 blocking antibody (10 µg/ml, clone MIAP410, mouse IgG1, κ; Cat. BE0283, BioXCell) and/or an anti-PD-L1 blocking antibody (Avelumab, Human IgG1, λ, Cat. SIM0021 BioXCell), which were maintained throughout the duration of the co-culture. To prevent antibody dependent cytotoxicity, NK cells were pre-incubated with human FcR Block (Cat. No. 130-092-575, 1:5 dilution; Miltenyi Biotec) for 2 hours at 37°C before their addition to target cells. NK cell activation was evaluated by measuring CD107a expression in $CD56^{+}$ cells as a marker of degranulation. Flow cytometry analysis was performed using a BD LSRFortessa™ Cell Analyzer. Data were analysed using FSC express 7 software.

Statistical Analyses

Statistical analyses were performed using Prism 11 (Graphpad). Detailed statistical analyses have been provided in the legend of each figure.

Clinical trial number: not applicable.

Human Ethics

All eye tissue was provided by NHS Blood and Transplant Tissue and Eye Services or the Newcastle NHS Trust following ethical approval from the NHS Research Ethics Committee (Title: Understanding the molecular and cellular complexity of adult human eye, 18/YH/04/20, approval date 29.10.2018). Whole blood was collected from healthy donors following informed consent, under approval no. 3031/56684 from the Newcastle University Ethics Committee (Title**:** Off-the-shelf hypoimmunogenic LSCs for treatment of limbal stem cell deficiency, approval date 1st July 2025)

Consent to Participate

Eyes from three adult human donors were donated for research, and whole blood samples were collected from healthy adult donors, with informed consent obtained in all cases.

Acknowledgements

The authors sincerely thank Julie Walsh from John Walton Research Centre and Dr. Nik Tzoumas for peripheral blood collections. The purchase of IncuCyte used in this study was supported by a UKRI MRC Capital Funding for World Class Labs Award (MR/X012360/1). This work was supported by Fight for Sight (Grant No. 5181/5182) and the UKRI Funding Guarantee (EP/Y031016/1). We would also like to thank Newcastle University Genomics, Bioimaging, and Flow Cytometry for their invaluable help during this study.

Funding Declaration

This work was supported by Fight for Sight (Grant No. 5181/5182) and the UKRI Funding Guarantee (EP/Y031016/1).

AI usage declaration

The text was reviewed using AI-assisted tools to improve grammar and readability.

Author Contributions

EG – study and experimental design, data collection and analyses, figure preparation, manuscript writing

SH, KM, GRS, BD, MM – data collection and analyses

SA, FCF – study design and fundraising

ML, LA – study and experimental design, figure preparation, manuscript writing, data dissemination, and fundraising

All authors approved the final version of this manuscript.

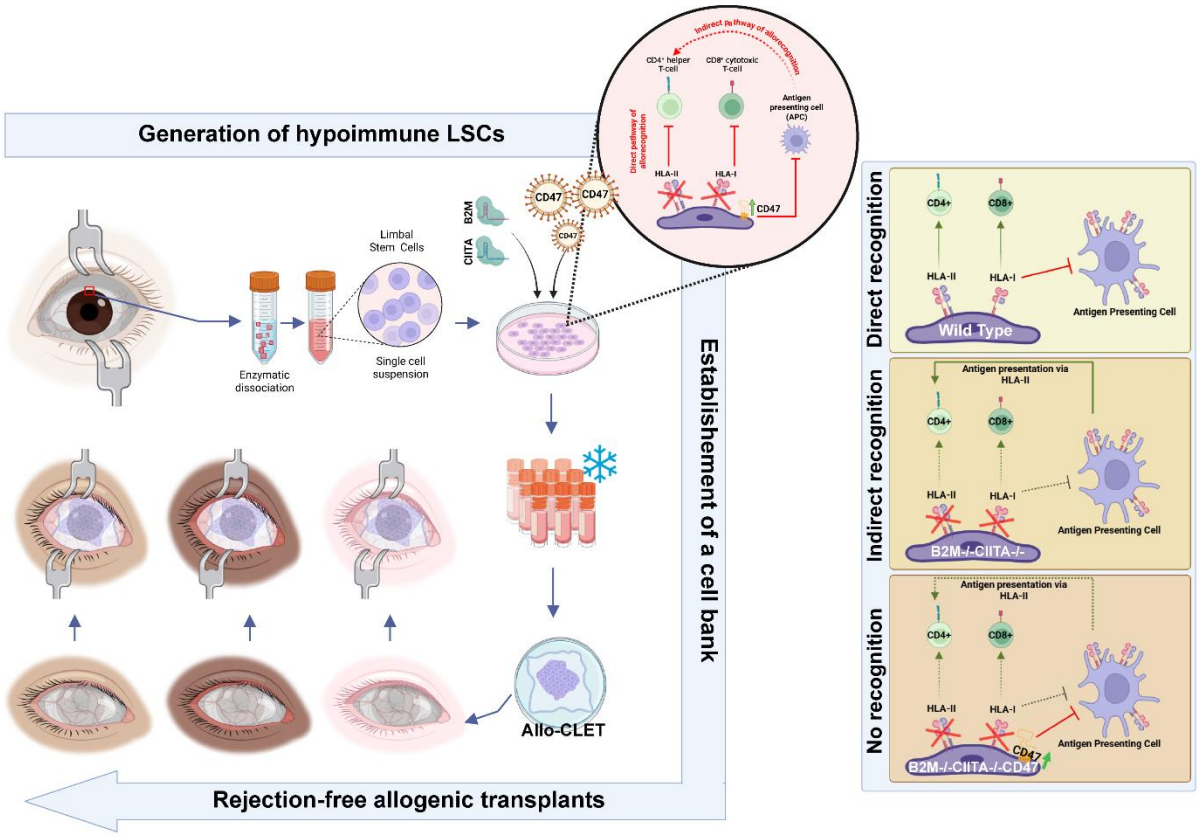
References

1. Dua HS, Azuara-Blanco A. Limbal stem cells of the corneal epithelium. Surv Ophthalmol. 2000 Mar-Apr;44(5):415-25.
2. Daniels JT, Dart JK, Tuft SJ, et al. Corneal stem cells in review. Wound Repair Regen. 2001 Nov-Dec;9(6):483-94.
3. Chen JJ, Tseng SC. Abnormal corneal epithelial wound healing in partial-thickness removal of limbal epithelium. Invest Ophthalmol Vis Sci. 1991 Jul;32(8):2219-33.
4. Dua HS, Saini JS, Azuara-Blanco A, et al. Limbal stem cell deficiency: concept, aetiology, clinical presentation, diagnosis and management. Indian J Ophthalmol. 2000 Jun;48(2):83-92.
5. Deng SX, Borderie V, Chan CC, et al. Global Consensus on Definition, Classification, Diagnosis, and Staging of Limbal Stem Cell Deficiency. Cornea. 2019 Mar;38(3):364-375.
6. Sangwan VS, Basu S, MacNeil S, et al. Simple limbal epithelial transplantation (SLET): a novel surgical technique for the treatment of unilateral limbal stem cell deficiency. Br J Ophthalmol. 2012 Jul;96(7):931-4.
7. Kenyon KR, Tseng SC. Limbal autograft transplantation for ocular surface disorders. Ophthalmology. 1989 May;96(5):709-22; discussion 722-3.
8. Holland EJ. Epithelial transplantation for the management of severe ocular surface disease. Trans Am Ophthalmol Soc. 1996;94:677-743.
9. Turgeon PW, Nauheim RC, Roat MI, et al. Indications for keratoepithelioplasty. Arch Ophthalmol. 1990 Feb;108(2):233-6.
10. Tsai RJ TS. Human allograft limbal transplantation for corneal surface reconstruction. Cornea. 1994;13(5).
11. Figueiredo GS, Salvador-Culla B, Baylis OJ, et al. Outcomes of Penetrating Keratoplasty Following Autologous Cultivated Limbal Epithelial Stem Cell Transplantation. Stem Cells. 2018 Jun;36(6):925-931.
12. Pellegrini G, Traverso CE, Franzi AT, et al. Long-term restoration of damaged corneal surfaces with autologous cultivated corneal epithelium. Lancet. 1997 Apr 5;349(9057):990-3.
13. Ramaesh K, Dhillon B. Ex vivo expansion of corneal limbal epithelial/stem cells for corneal surface reconstruction. Eur J Ophthalmol. 2003 Jul;13(6):515-24.
14. Shortt AJ, Secker GA, Notara MD, et al. Transplantation of ex vivo cultured limbal epithelial stem cells: a review of techniques and clinical results. Surv Ophthalmol. 2007 Sep-Oct;52(5):483-502.
15. Jackson CJ MEI, Ringstad H, Tønseth KA, Dartt DA, Utheim TP. Simple limbal epithelial transplantation: Current status and future perspectives. Stem Cells Translational Medicine. 2020;9(3):316-327.
16. Kolli S AS, Mudhar HS, Meeny A, Lako M, Figueiredo FC. Successful application of ex vivo expanded human autologous oral mucosal epithelium for the treatment of total bilateral limbal stem cell deficiency. Stem Cells. 2014;32(8):2135-46.
17. Rao SK RR, Sitalakshmi G, Padmanabhan P. Limbal allografting from related live donors for corneal surface reconstruction. Ophthalmology. 1999;106(4).
18. Rama P MS, Paganoni G, Spinelli A, De Luca M, Pellegrini G. Limbal stem-cell therapy and long-term corneal regeneration. N Engl J Med. 2010;363(2):147-55.
19. Bakhtiari P DA. Update on limbal stem cell transplantation. Middle East Afr J Ophthalmol. 2010;17(1):9-14.
20. Ghareeb AE LM, Figueiredo FC. Recent Advances in Stem Cell Therapy for Limbal Stem Cell Deficiency: A Narrative Review. Ophthalmol Ther. 2020;9(4):809-831.

21. Behaegel J ZN, Tassignon MJ, Leysen I, Bock F, Koppen C, Ní Dhubhghaill S. Short- and Long-Term Results of Xenogeneic-Free Cultivated Autologous and Allogeneic Limbal Epithelial Stem Cell Transplantations. Cornea. 2019;38(12):1543-1549.
22. Galo E, Figueiredo FC, Lako M, et al. Implementing stem-cell therapies for limbal stem cell deficiency. Regen Med. 2026 Feb;21(2):155-162.
23. Han X, Wang M, Duan S, et al. Generation of hypoimmunogenic human pluripotent stem cells. Proc Natl Acad Sci U S A. 2019 May 21;116(21):10441-10446.
24. Deuse T, Hu X, Gravina A, et al. Hypoimmunogenic derivatives of induced pluripotent stem cells evade immune rejection in fully immunocompetent allogeneic recipients. Nat Biotechnol. 2019 Mar;37(3):252-258.
25. Hu X, White K, Olroyd AG, et al. Hypoimmune induced pluripotent stem cells survive long term in fully immunocompetent, allogeneic rhesus macaques. Nat Biotechnol. 2024 Mar;42(3):413-423.
26. Deuse T, Hu X, Agbor-Enoh S, et al. The SIRPalpha-CD47 immune checkpoint in NK cells. J Exp Med. 2021 Mar 1;218(3).
27. Gravina A, Tediashvili G, Rajalingam R, et al. Protection of cell therapeutics from antibody-mediated killing by CD64 overexpression. Nat Biotechnol. 2023 May;41(5):717-727.
28. Hu X, Tediashvili G, Gravina A, et al. Inhibition of polymorphonuclear cells averts cytotoxicity against hypoimmune cells in xenotransplantation. Nat Commun. 2025 Apr 18;16(1):3706.
29. Carlsson PO, Hu X, Scholz H, et al. Survival of Transplanted Allogeneic Beta Cells with No Immunosuppression. N Engl J Med. 2025 Sep 4;393(9):887-894.
30. Neelapu SS, Budde LE, McGuirk JP, et al. Phase 1 Study of SC291, a Hypoimmune, Allogeneic CD19-Directed CAR T Cell Therapy for Relapsed/Refractory B-Cell Malignancies (ARDENT) - Initial Clinical Data. Blood. 2023;142(Supplement 1):6852-6852.
31. Miyashita H, Yokoo S, Yoshida S, et al. Long-term maintenance of limbal epithelial progenitor cells using rho kinase inhibitor and keratinocyte growth factor. Stem Cells Transl Med. 2013 Oct;2(10):758-65.
32. Sun CC, Chiu HT, Lin YF, et al. Y-27632, a ROCK Inhibitor, Promoted Limbal Epithelial Cell Proliferation and Corneal Wound Healing. PLoS One. 2015;10(12):e0144571.
33. Wu X, Wang S, Li M, et al. Conditional reprogramming: next generation cell culture. Acta Pharm Sin B. 2020 Aug;10(8):1360-1381.
34. Zhou Q, Duan H, Wang Y, et al. ROCK inhibitor Y-27632 increases the cloning efficiency of limbal stem/progenitor cells by improving their adherence and ROS-scavenging capacity. Tissue Eng Part C Methods. 2013 Jul;19(7):531-7.
35. Catala P, Groen N, Dehnen JA, et al. Single cell transcriptomics reveals the heterogeneity of the human cornea to identify novel markers of the limbus and stroma. Sci Rep. 2021 Nov 5;11(1):21727.
36. Collin J, Queen R, Zerti D, et al. A single cell atlas of human cornea that defines its development, limbal progenitor cells and their interactions with the immune cells. Ocul Surf. 2021 Jul;21:279-298.
37. Freibaum JS, Leathem RP, Braaton W, et al. Unraveling CD8(+) T cell alloimmunity: Insights into the direct pathway of antigen recognition from modern experimental tools. Am J Transplant. 2025 Sep;25(9):1843-1850.
38. Morandi F, Pistoia V. Interactions between HLA-G and HLA-E in Physiological and Pathological Conditions. Front Immunol. 2014;5:394.
39. Moretta A, Bottino C, Vitale M, et al. Activating receptors and coreceptors involved in human natural killer cell-mediated cytolysis. Annu Rev Immunol. 2001;19:197-223.
40. Beers C, Ilaria RL, Luke JJ. Unlocking the promise of innate biology through the HLA-G/ILT2/ILT4 pathway. J Immunother Cancer. 2026 Feb 15;14(2).

41. Poncette L, Bluhm J, Blankenstein T. The role of CD4 T cells in rejection of solid tumors. Curr Opin Immunol. 2022 Feb;74:18-24.
42. Boisgerault F, Liu Y, Anosova N, et al. Differential roles of direct and indirect allorecognition pathways in the rejection of skin and corneal transplants. Transplantation. 2009 Jan 15;87(1):16-23.
43. Siu JHY, Surendrakumar V, Richards JA, et al. T cell Allorecognition Pathways in Solid Organ Transplantation. Front Immunol. 2018;9:2548.
44. Oldenborg PA, Zheleznyak A, Fang YF, et al. Role of CD47 as a marker of self on red blood cells. Science. 2000 Jun 16;288(5473):2051-4.
45. Blank C, Mackensen A. Contribution of the PD-L1/PD-1 pathway to T-cell exhaustion: an update on implications for chronic infections and tumor evasion. Cancer Immunol Immunother. 2007 May;56(5):739-45.
46. Gordon SR, Maute RL, Dulken BW, et al. PD-1 expression by tumour-associated macrophages inhibits phagocytosis and tumour immunity. Nature. 2017 May 25;545(7655):495-499.
47. Kennedy A, Waters E, Rowshanravan B, et al. Differences in CD80 and CD86 transendocytosis reveal CD86 as a key target for CTLA-4 immune regulation. Nat Immunol. 2022 Sep;23(9):1365-1378.
48. Dugger K, Lowder TW, Tucker TA, et al. Epithelial cells as immune effector cells: the role of CD40. Semin Immunol. 2009 Oct;21(5):289-92.
49. Saha S, Haynes WJ, Del Rio NM, et al. Diminished Immune Cell Adhesion in Hypoimmune ICAM-1 Knockout Pluripotent Stem Cells. bioRxiv. 2024 Jun 9.
50. Morrissey MA, Kern N, Vale RD. CD47 Ligation Repositions the Inhibitory Receptor SIRPA to Suppress Integrin Activation and Phagocytosis. Immunity. 2020 Aug 18;53(2):290-302 e6.
51. Feng Y, Huang C, Wang Y, et al. SIRPalpha: A key player in innate immunity. Eur J Immunol. 2023 Nov;53(11):e2350375.
52. Barcelo J, Samain R, Sanz-Moreno V. Preclinical to clinical utility of ROCK inhibitors in cancer. Trends Cancer. 2023 Mar;9(3):250-263.
53. Galo E, Figueiredo F, Ali S, et al. Long-term maintenance of adult limbal epithelial stem cells (LSC) using Rock Inhibitor and assessment of its effects on cell identity. Investigative Ophthalmology & Visual Science. 2024;65(7):2006-2006.
54. Kahuam-Lopez N, Yeung SN, Iovieno A. Resolution of limbal stem cell deficiency with the use of a topical Rho kinase inhibitor. Can J Ophthalmol. 2024 Jun;59(3):e271-e272.
55. Terheyden-Keighley D, Huhne M, Berger T, et al. GMP-compliant iPS cell lines show widespread plasticity in a new set of differentiation workflows for cell replacement and cancer immunotherapy. Stem Cells Transl Med. 2024 Sep 10;13(9):898-911.
56. Kinoshita S, Koizumi N, Ueno M, et al. Injection of Cultured Cells with a ROCK Inhibitor for Bullous Keratopathy. N Engl J Med. 2018 Mar 15;378(11):995-1003.
57. Zhang Q, Chen H, Cun J, et al. A simple and standardized method supports efficient derivation of clinical-grade human embryonic stem cells under feeder- and xeno-free conditions. Stem Cell Res Ther. 2025 Dec 1;17(1):9.
58. Gornalusse GG, Hirata RK, Funk SE, et al. HLA-E-expressing pluripotent stem cells escape allogeneic responses and lysis by NK cells. Nat Biotechnol. 2017 Aug;35(8):765-772.
59. Guo Y, Xu B, Wu Z, et al. Mutant B2M-HLA-E and B2M-HLA-G fusion proteins protects universal chimeric antigen receptor-modified T cells from allogeneic NK cell-mediated lysis. Eur J Immunol. 2021 Oct;51(10):2513-2521.
60. Shi L, Li W, Liu Y, et al. Generation of hypoimmunogenic human pluripotent stem cells via expression of membrane-bound and secreted beta2m-HLA-G fusion proteins. Stem Cells. 2020 Nov;38(11):1423-1437.

61. Dhatchinamoorthy K, Colbert JD, Rock KL. Cancer Immune Evasion Through Loss of MHC Class I Antigen Presentation. Front Immunol. 2021;12:636568.
62. Treseler PA, Foulks GN, Sanfilippo F. Expression of ABO blood group, hematopoietic, and other cell-specific antigens by cells in the human cornea. Cornea. 1985;4(3):157-68.
63. Dua HS, Shidham VB. Application of specific red blood cell adherence test to the human cornea and conjunctiva. Am J Ophthalmol. 1979 Dec;88(6):1067-71.
64. Chan JH, Dua HS, Powell-Richards A, et al. Effect of ABO blood group mismatching on corneal epithelial cells: an in vitro study. Br J Ophthalmol. 2001 Sep;85(9):1104-9.
65. Tan JC, Wadia PP, Coram M, et al. H-Y antibody development associates with acute rejection in female patients with male kidney transplants. Transplantation. 2008 Jul 15;86(1):75-81.
66. Foulsham W, Coco G, Amouzegar A, et al. When Clarity Is Crucial: Regulating Ocular Surface Immunity. Trends Immunol. 2018 Apr;39(4):288-301.



Graphical Abstract

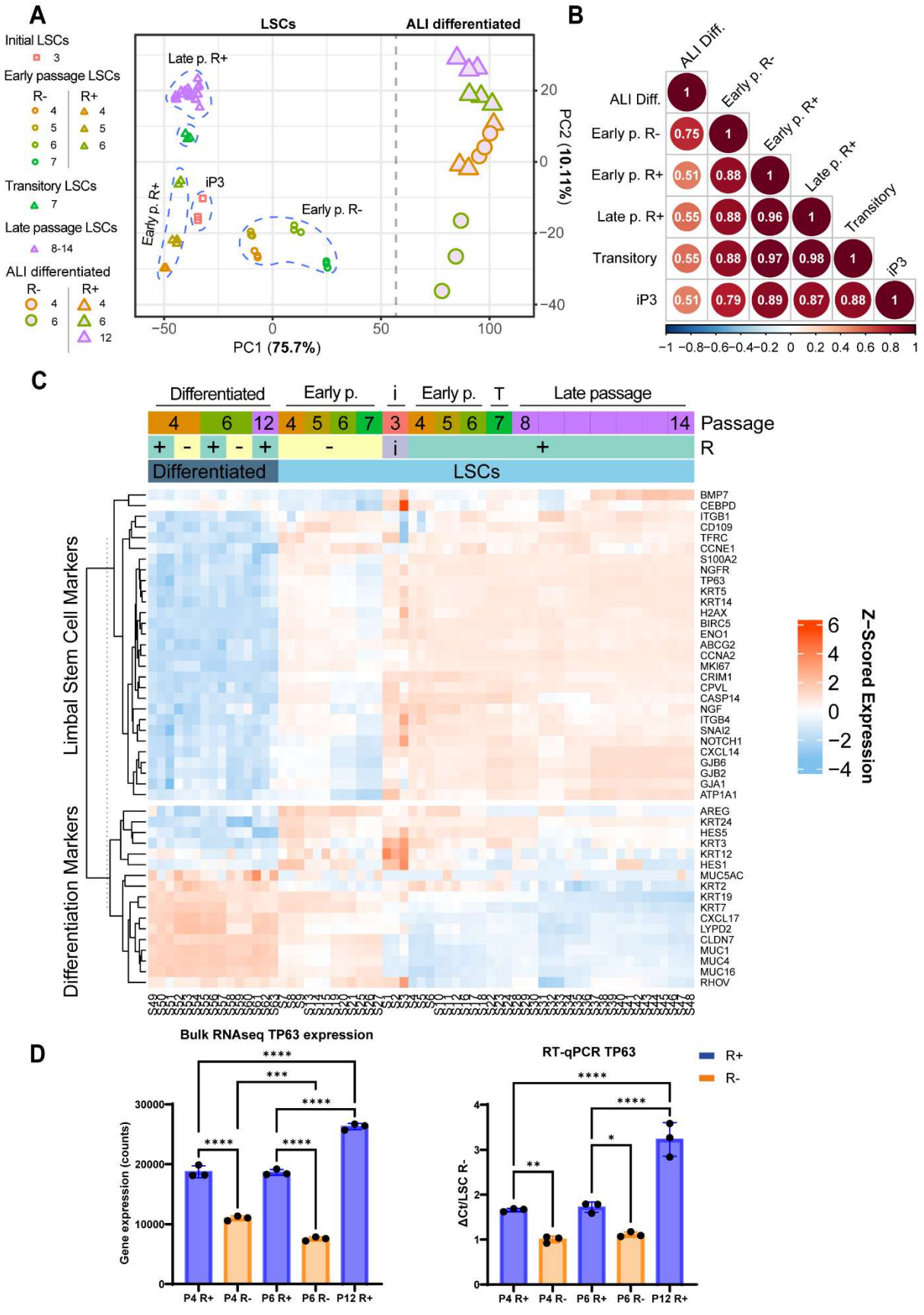

A
Initial LSCs
3
Early passage LSCs
R-
4
5
6
7
R+
4
5
6
Transitory LSCs
7
Late passage LSCs
8-14
ALI differentiated
R-
4
6
R+
4
6
12
LSCs
ALI differentiated
Late p. R+
iP3
Early p. R+
Early p. R-
PC1 (75.7%)
PC2 (10.11%)
B
ALI Diff.
Early p. R-
Early p. R+
Late p. R+
Transitory
iP3
C
Differentiated
Early p.
i
Early p.
T
Late passage
Passage
R
Differentiated
LSCs
Limbal Stem Cell Markers
Differentiation Markers
BMP7
CEBPD
ITGB1
CD109
TFRC
CCNE1
S100A2
NGFR
TP63
KRT5
KRT14
H2AX
BIRC5
ENO1
ABCG2
CCNA2
MKI67
CRIM1
CPVL
CASP14
NGF
ITGB4
SNAI2
NOTCH1
CXCL14
GJB6
GJB2
GJA1
ATP1A1
AREG
KRT24
HES5
KRT3
KRT12
HES1
MUC5AC
KRT2
KRT19
KRT7
CXCL17
LYPD2
CLDN7
MUC1
MUC4
MUC16
RHOV
Z-Scored Expression
D
Bulk RNAseq TP63 expression
Gene expression (counts)
P4 R+
P4 R-
P6 R+
P6 R-
P12 R+
RT-qPCR TP63
R+
R-
ΔCt/LSC R-

Figure 1: Transcriptional landscape of LSCs and ALI-differentiated derivatives across serial passage.

(A) Principal component analysis (PCA) of bulk RNA-seq gene expression data from initial LSCs (iP3), R- LSCs (P4-P7), R+ LSCs (P4-P14), and ALI-differentiated derivatives (P4 R-, P4 R+, P6 R-, P6 R+, P12 R+). Samples were grouped into five clusters based on PCA distribution: initial, early-passage, transitory, late-passage, and ALI-differentiated (demarcated by blue dashed lines)**.** The square denotes iP3; small circles, R- LSCs; small triangles, R+ LSCs; large, filled symbols, ALI-differentiated samples. Large circles represent R- derived ALI samples; large triangles, R+ derived ALI samples. Numbers indicate passages. R+ and R- correspond to cultures with or without ROCK inhibitor (Ri), respectively. **(B)** Pairwise correlation analysis of the defined transcriptional clusters. **(C)** Heatmap of Z-scored expression of established LSC and corneal differentiation markers across all samples, with passage numbers indicated. **(D)** Validation of the key LSC marker *TP63* by qPCR.

All panels: Data are from three replicates. Panel (D): Statistical analysis was performed using one-way ANOVA with multiple comparisons followed by Tukey's multiple comparison test. in. * $p < 0.05$; ** $p < 0.01$; *** $p < 0.001$; **** $p < 0.0001$.

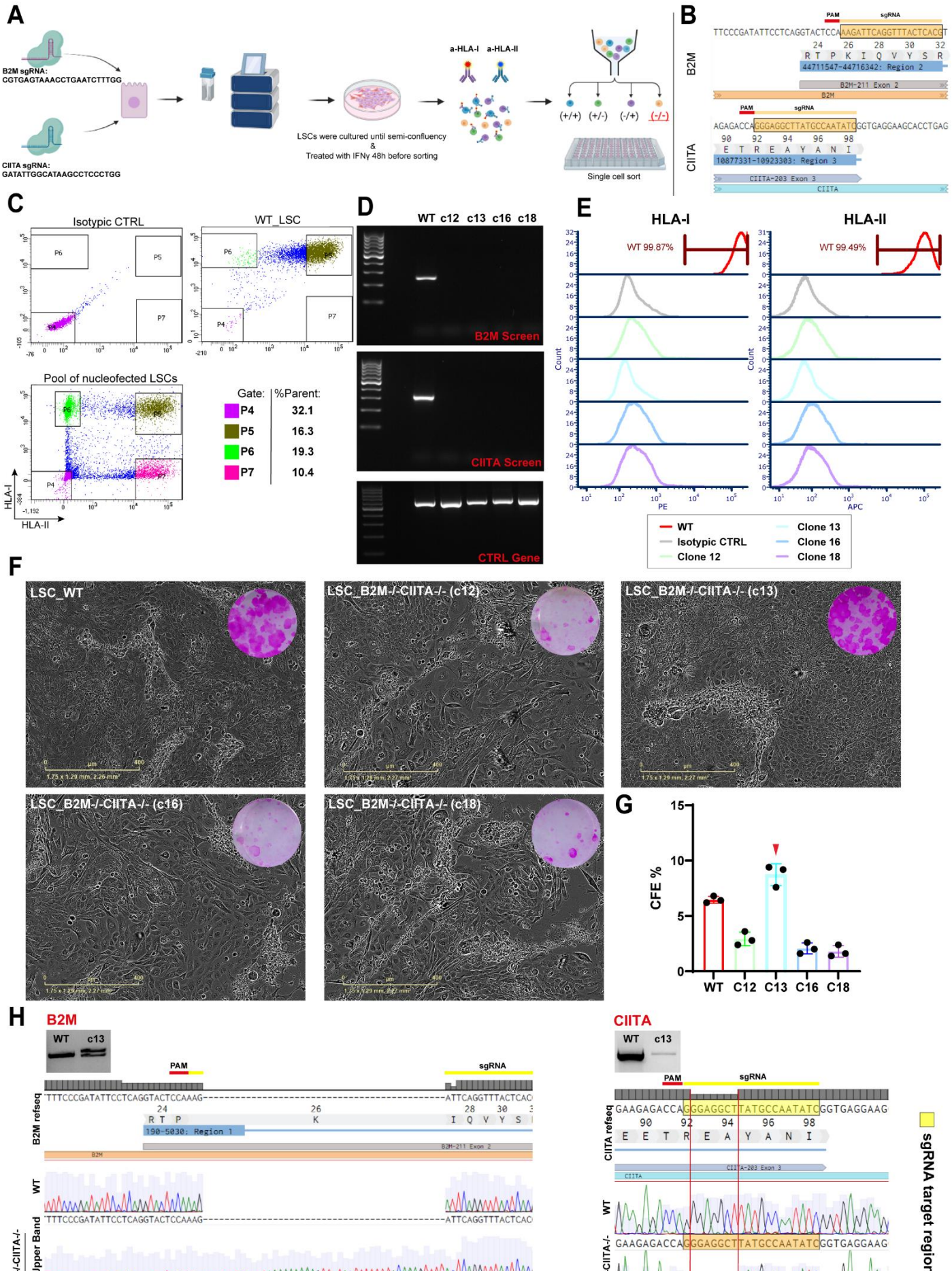
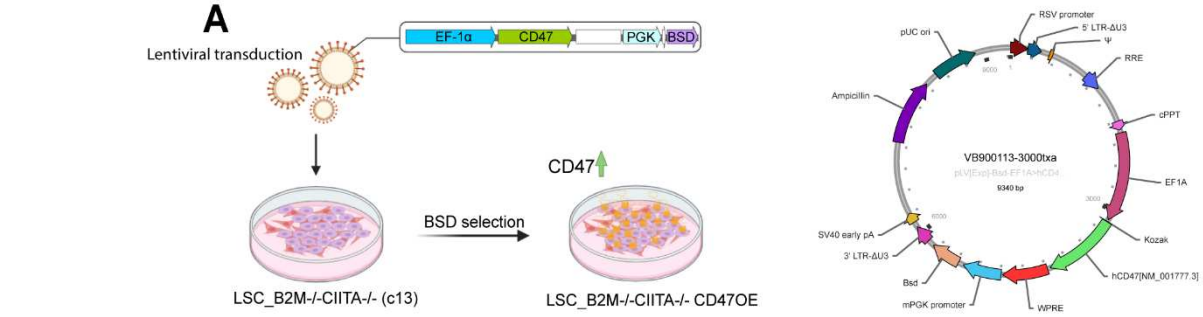
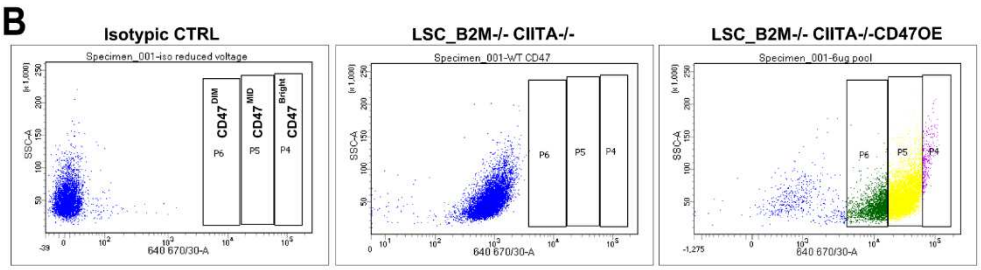
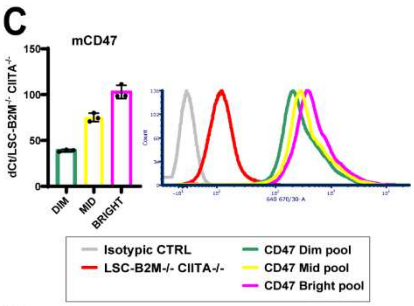

A
B2M sgRNA:
CGTGAGTAAACCTGAATCTTTGG
CIITA sgRNA:
GATATTGGCATAAGCCTCCCTGG
LSCs were cultured until semi-confluency
&
Treated with IFNγ 48h before sorting
a-HLA-I
a-HLA-II
(+/+)
(+/-)
(-/+)
(-/-)
Single cell sort
B
B2M
CIITA
PAM
sgRNA
C
Isotypic CTRL
WT_LSC
Pool of nucleofected LSCs
HLA-I
HLA-II
Gate:
%Parent:
P4 32.1
P5 16.3
P6 19.3
P7 10.4
D
WT c12 c13 c16 c18
B2M Screen
CIITA Screen
CTRL Gene
E
HLA-I
HLA-II
WT 99.87%
WT 99.49%
Count
PE
APC
WT
Isotypic CTRL
Clone 12
Clone 13
Clone 16
Clone 18
F
LSC_WT
LSC_B2M-/-CIITA-/- (c12)
LSC_B2M-/-CIITA-/- (c13)
LSC_B2M-/-CIITA-/- (c16)
LSC_B2M-/-CIITA-/- (c18)
G
CFE %
WT C12 C13 C16 C18
H
B2M
CIITA
WT c13
B2M refseq
CIITA refseq
WT
LSC_B2M-/-CIITA-/-
Upper Band
Lower Band
sgRNA target region

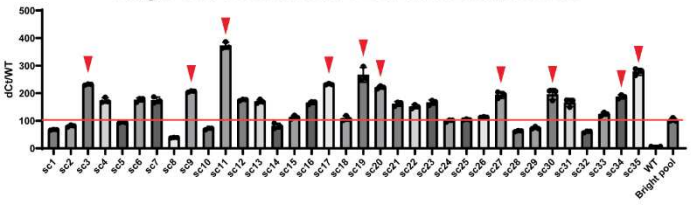
Figure 2: Generation of HLA-I and HLA-II ablated LSCs.

(A) Schematic overview of the dual-knockout strategy targeting *B2M* & *CIITA*. **(B)** Genomic region targeted by *B2M* and *CIITA* sgRNAs. **(C)** Flow cytometric isolation of HLA-I^{-} and HLA-II^{-} cells from the nucleofected LSC pool by single-cell sorting. **(D)** PCR-based screening for indel introduction at the *B2M* and *CIITA* cut sites across individual clones. **(E)** Flow cytometric validation of HLA-I and HLA-II surface expression in PCR-confirmed indel-bearing clones (c12, c13, c16, c18). **(F)** Representative brightfield images of *B2M*$^{-/-}$*CIITA*$^{-/-}$ LSC clones illustrating colony morphology and whole well CFE. Scale bar, 400 µm. **(G)** CFE of *B2M*$^{-/-}$*CIITA*$^{-/-}$ LSC clones, with clone 13 displaying higher clonogenic capacity. **(H)** Sanger sequencing confirming biallelic indels at the *B2M* and *CIITA* cut sites in clone 13.





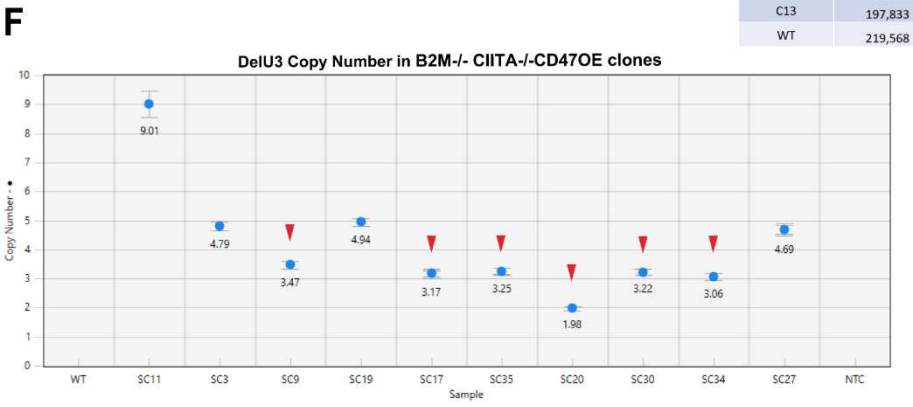


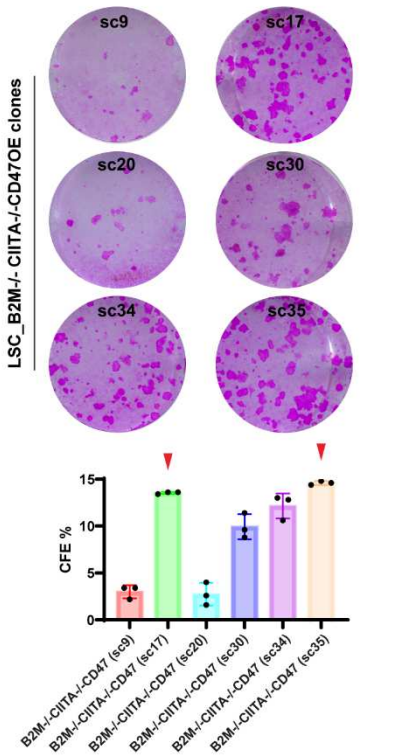


E

a-CD47 bound/cell

Clone	PE mol/cell
c13-SC11	6,962,165
c13-SC35	3,228,144
c13-SC19	5,181,907
c13-SC17	2,900,254
c13-SC3	4,421,329
c13-SC20	3,308,510
c13-SC9	3,004,542
c13-SC30	4,227,500
c13-SC27	2,632,919
c13-SC34	3,389,685
C13	197,833
WT	219,568





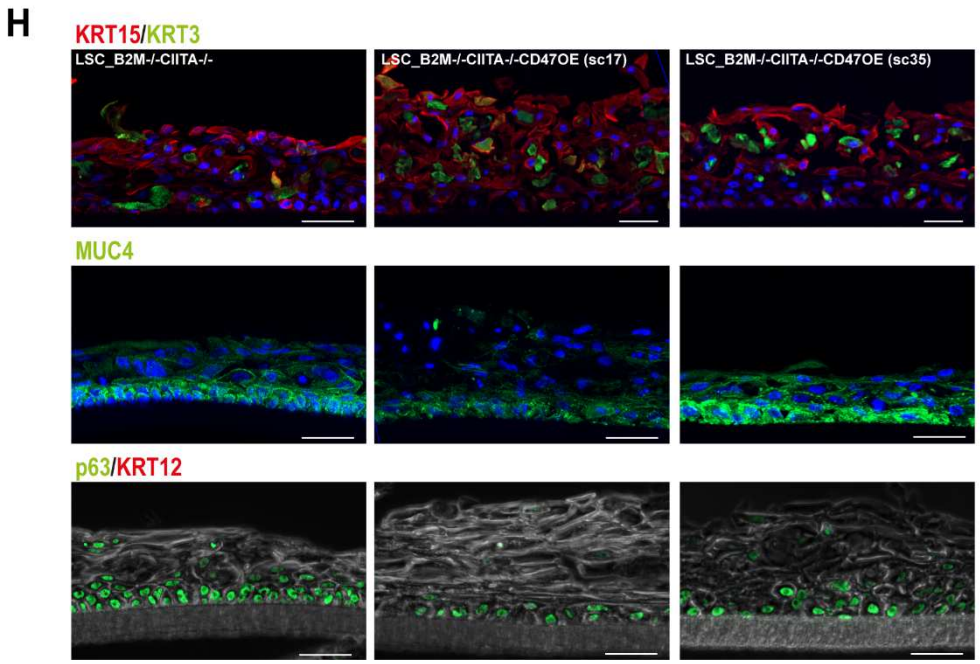


Figure 3: Overexpression of the CD47 immune checkpoint inhibitor in HLA-I and HLA-II ablated LSCs.

(A) Schematic representation of the lentiviral construct harbouring the *CD47* transgene under the transcriptional control of the constitutive *EF1α* promoter. The vector incorporates a blasticidin resistance marker to facilitate the selection and enrichment of stably transduced LSCs. **(B)** Flow Cytometric Profiling and Sorting of CD47-Transduced LSCs. Representative histograms showing CD47 surface expression in transduced versus non-transduced LSC clones following blasticidin selection. The gating strategy illustrates the demarcation of three distinct sub-populations based on fluorescence intensity: CD47-DIM (P6), CD47-MID (P5), and CD47-BRIGHT (P4), which were subsequently isolated via fluorescence-activated cell sorting (FACS). **(C)** Validation of CD47 overexpression in sorted cell populations by *CD47* mRNA quantification and flow cytometry. **(D)** Screening of single-cell clones isolated from the CD47 BRIGHT population for *CD47* mRNA expression, identifying the top ten candidates (sc3, sc9, sc11, sc17, sc19, sc20, sc27, sc30, sc34, sc35). **(E)** Quantitative flow cytometry using antibody-binding capacity (ABC) to determine CD47 protein expression levels across the top ten clones. (**F**) Droplet ddPCR quantification of viral copy number (VCN) per clone. **(G)** Colony-forming efficiency (CFE) assessment of clones with the lowest viral copy number (sc9, sc17, sc20, sc30, sc34, sc35), identifying clones 17 and 35 as having superior clonogenic capacity. **(H)** Immunofluorescence characterisation of stratification and ALI differentiation capacity in selected clones, assessed by expression of stem cell markers (p63, KRT15) and differentiation markers (KRT3, KRT12, MUC4). Scale bar, 50 μm.

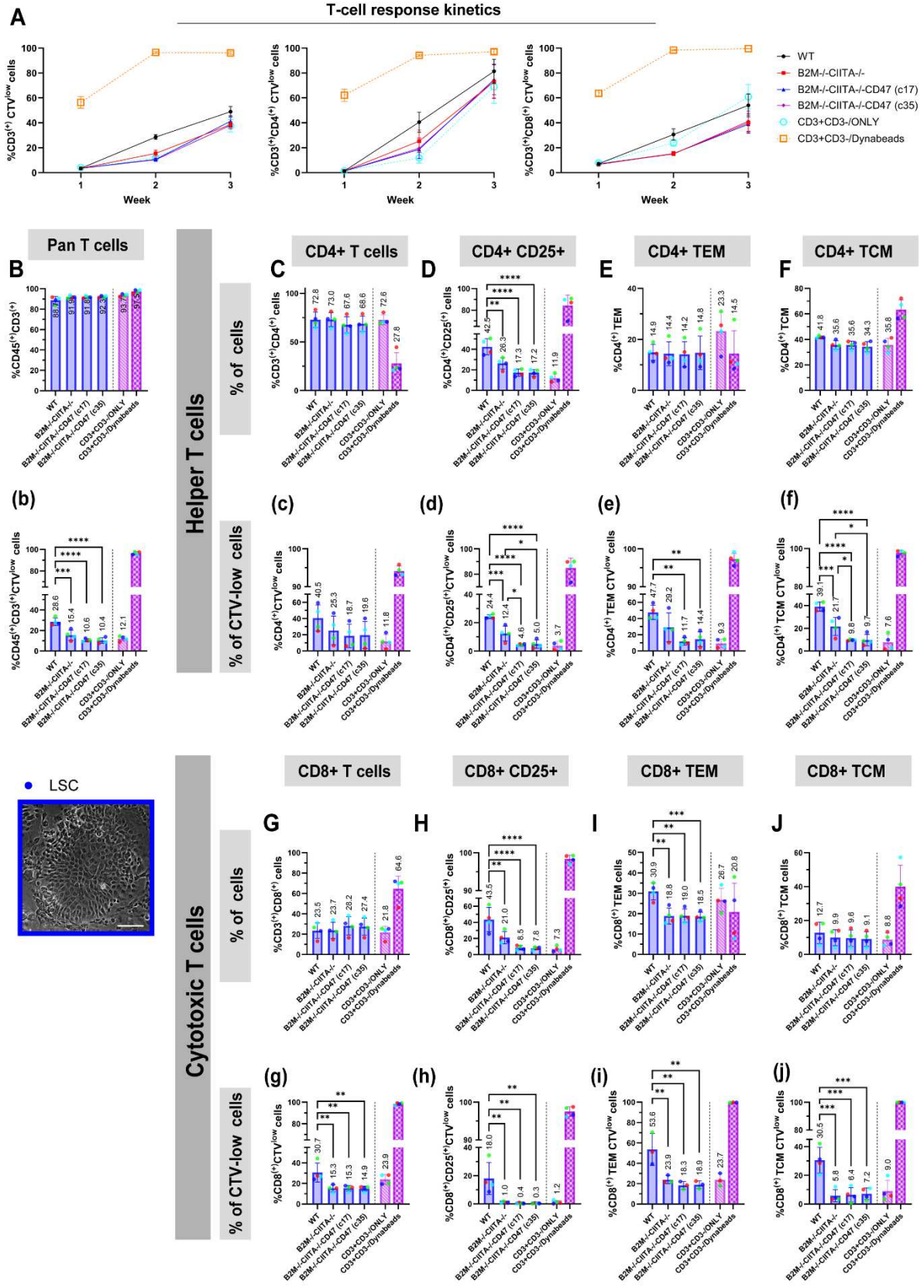
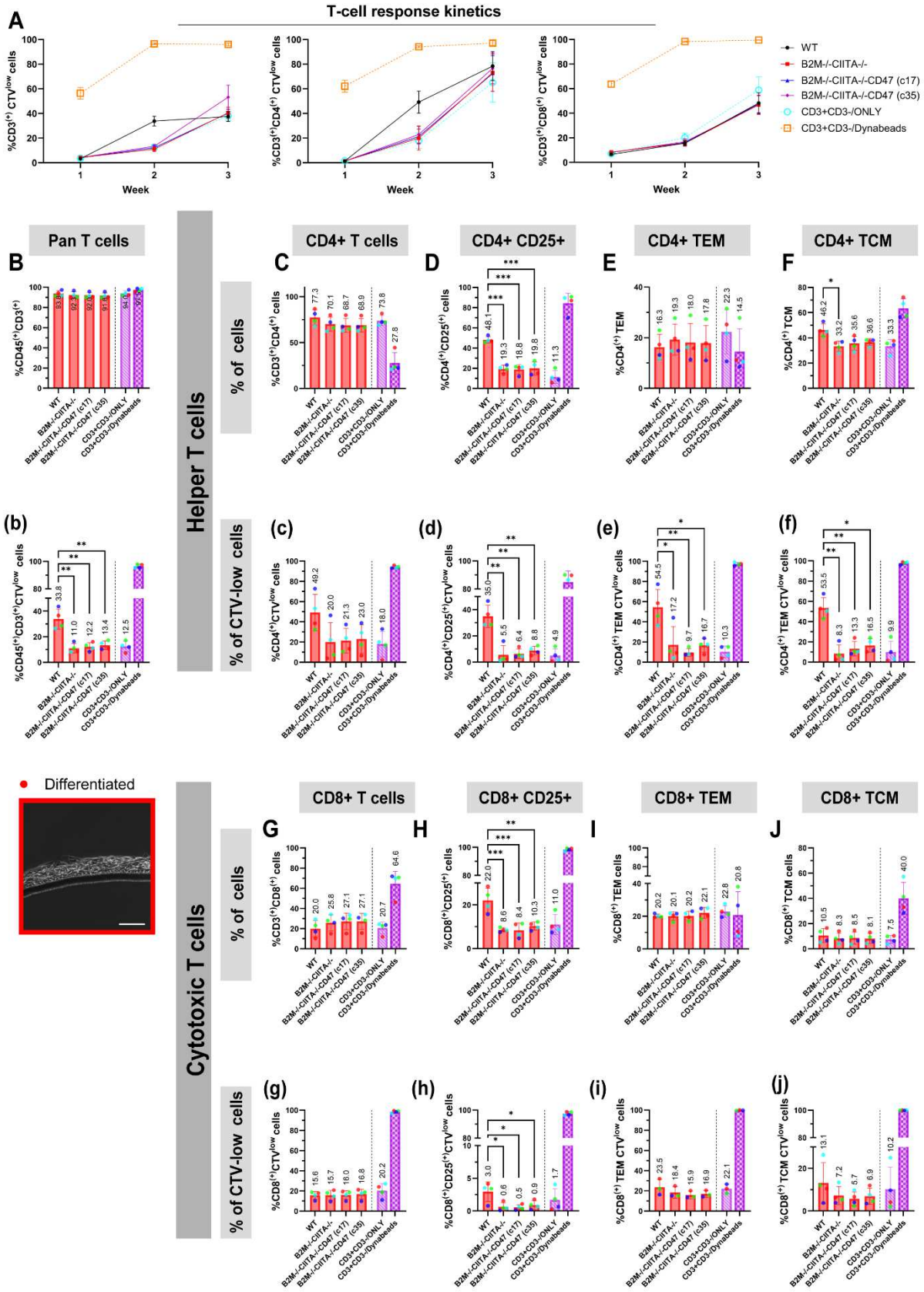

A
T-cell response kinetics
%CD3(+) CTVlow cells
%CD3(+)CD4(+) CTVlow cells
%CD3(+)CD8(+) CTVlow cells
Week
WT
B2M-/-CIITA-/-
B2M-/-CIITA-/-CD47 (c17)
B2M-/-CIITA-/-CD47 (c35)
CD3+CD3-/ONLY
CD3+CD3-/Dynabeads
Pan T cells
CD4+ T cells
CD4+ CD25+
CD4+ TEM
CD4+ TCM
Helper T cells
% of cells
% of CTV-low cells
CD8+ T cells
CD8+ CD25+
CD8+ TEM
CD8+ TCM
Cytotoxic T cells
LSC

Figure 4: CD47 overexpressing B2M-/-CIITA-/- LSCs evade T cell allorecognition.

WT, B2M$^{-/-}$CIITA$^{-/-}$, and B2M$^{-/-}$CIITA$^{-/-}$CD47OE LSC clones were co-cultured with T cells isolated from four independent donors, and allogeneic T cell activation and proliferation were monitored by flow cytometry at weekly intervals over a three-week period. **(A)** Longitudinal assessment of pan (CD3+), helper (CD4+), and cytotoxic (CD8+) T cell proliferation across three weeks of co-culture. Week 2, which represented the optimal experimental time point for discriminating differential allogeneic responses across conditions, was selected for detailed phenotypic analysis of T cell subpopulations. Percentage of population and proliferation index are shown for **(B, b)** pan T cells, **(C, c)** helper T cells (CD4+), **(D, d)** activated helper T cells (Cd4+CD25+), **(E, e)** effector memory helper T cells (CD4+ TEM), and **(F, f)** central memory helper T cells (CD4+ TCM). Corresponding analyses for the cytotoxic T cell compartment are shown for **(G, g)** cytotoxic T cells (CD8+), **(H, h)** activated cytotoxic T cells (CD8+CD25+), **(I, i)** effector memory cytotoxic T cells (CD8+ TEM), and **(J, j)** central memory cytotoxic T cells (CD8+ TCM).

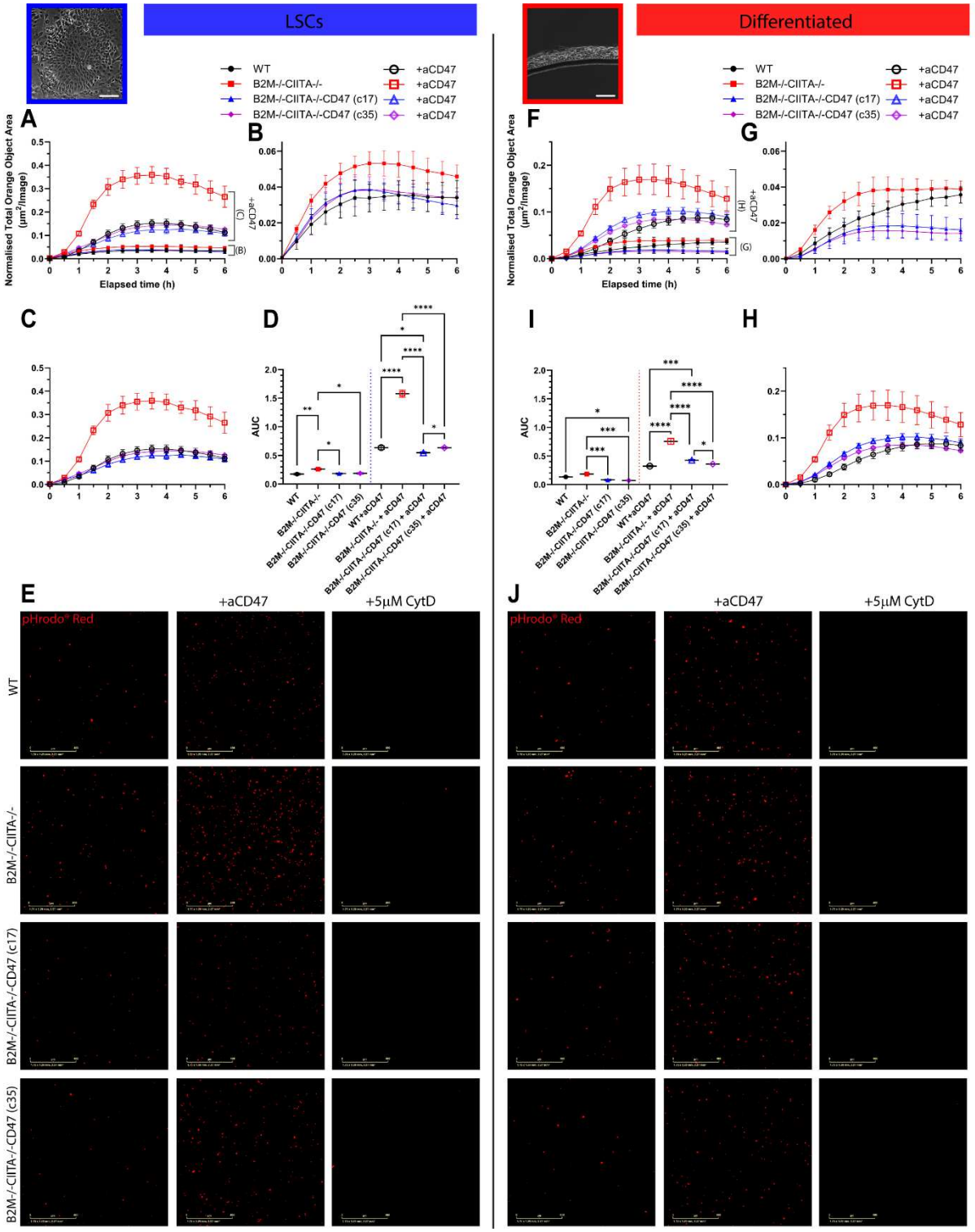
All panels: Data shown as mean ± *SD, (n=4)*. Statistical analysis was performed using one-way ANOVA with multiple comparisons followed by Tukey's multiple comparison test. * $p < 0.05$; ** $p < 0.01$; *** $p < 0.001$; **** $p < 0.0001$.


A
T-cell response kinetics
%CD3(+) CTV(low) cells
%CD3(+)CD4(+) CTV(low) cells
%CD3(+)CD8(+) CTV(low) cells
Week
WT
B2M-/-CIITA-/-
B2M-/-CIITA-/-CD47 (c17)
B2M-/-CIITA-/-CD47 (c35)
CD3+CD3-/ONLY
CD3+CD3-/Dynabeads
Helper T cells
% of cells
% of CTV-low cells
B
Pan T cells
%CD45(+)CD3(+)
C
CD4+ T cells
%CD3(+)CD4(+) cells
D
CD4+ CD25+
%CD4(+)CD25(+) cells
E
CD4+ TEM
%CD4(+) TEM
F
CD4+ TCM
%CD4(+) TCM
(b)
%CD45(+)CD3(+)CTV(low) cells
(c)
%CD4(+)CTV(low) cells
(d)
%CD4(+)CD25(+)CTV(low) cells
(e)
%CD4(+) TEM CTV(low) cells
(f)
%CD4(+) TEM CTV(low) cells
Differentiated
Cytotoxic T cells
% of cells
% of CTV-low cells
G
CD8+ T cells
%CD3(+)CD8(+) cells
H
CD8+ CD25+
%CD8(+)CD25(+) cells
I
CD8+ TEM
%CD8(+) TEM cells
J
CD8+ TCM
%CD8(+) TCM cells
(g)
%CD8(+)CTV(low) cells
(h)
%CD8(+)CD25(+)CTV(low) cells
(i)
%CD8(+) TEM CTV(low) cells
(j)
%CD8(+) TCM CTV(low) cells

1577

Figure 5: T cell response in cocultures with ALI- derived cells. WT, *B2M*$^{-/-}$*CIITA*$^{-/-}$, and *B2M*$^{-/-}$*CIITA*$^{-/-}$CD47OE ALI-derived cells were co-cultured with T cells isolated from four independent donors, and allogeneic T cell activation and proliferation were monitored by flow cytometry at weekly intervals over three weeks. **(A)** Longitudinal assessment of pan (CD3+), helper (CD4+), and cytotoxic (CD8+) T cell proliferation across three weeks of co-culture. Data are mean ± *SD*. Week 2, which represented the optimal experimental time point for discriminating differential allogeneic responses across conditions, was selected for detailed phenotypic analysis of T cell subpopulations. Percentage of population and proliferation index are shown for **(B, b)** pan T cells, **(C, c)** helper T cells (CD4+), **(D, d)** activated helper T cells (CD4+CD25+), **(E, e)** effector memory helper T cells (CD4+ TEM), and **(F, f)** central memory helper T cells (CD4+ TCM). Corresponding analyses for the cytotoxic T cell compartment are shown for **(G, g)** cytotoxic T cells (CD8+), **(H, h)** activated cytotoxic T cells (CD8+CD25+), **(I, i)** effector memory cytotoxic T cells (CD8+ TEM), and **(J, j)** central memory cytotoxic T cells (CD8+ TCM).

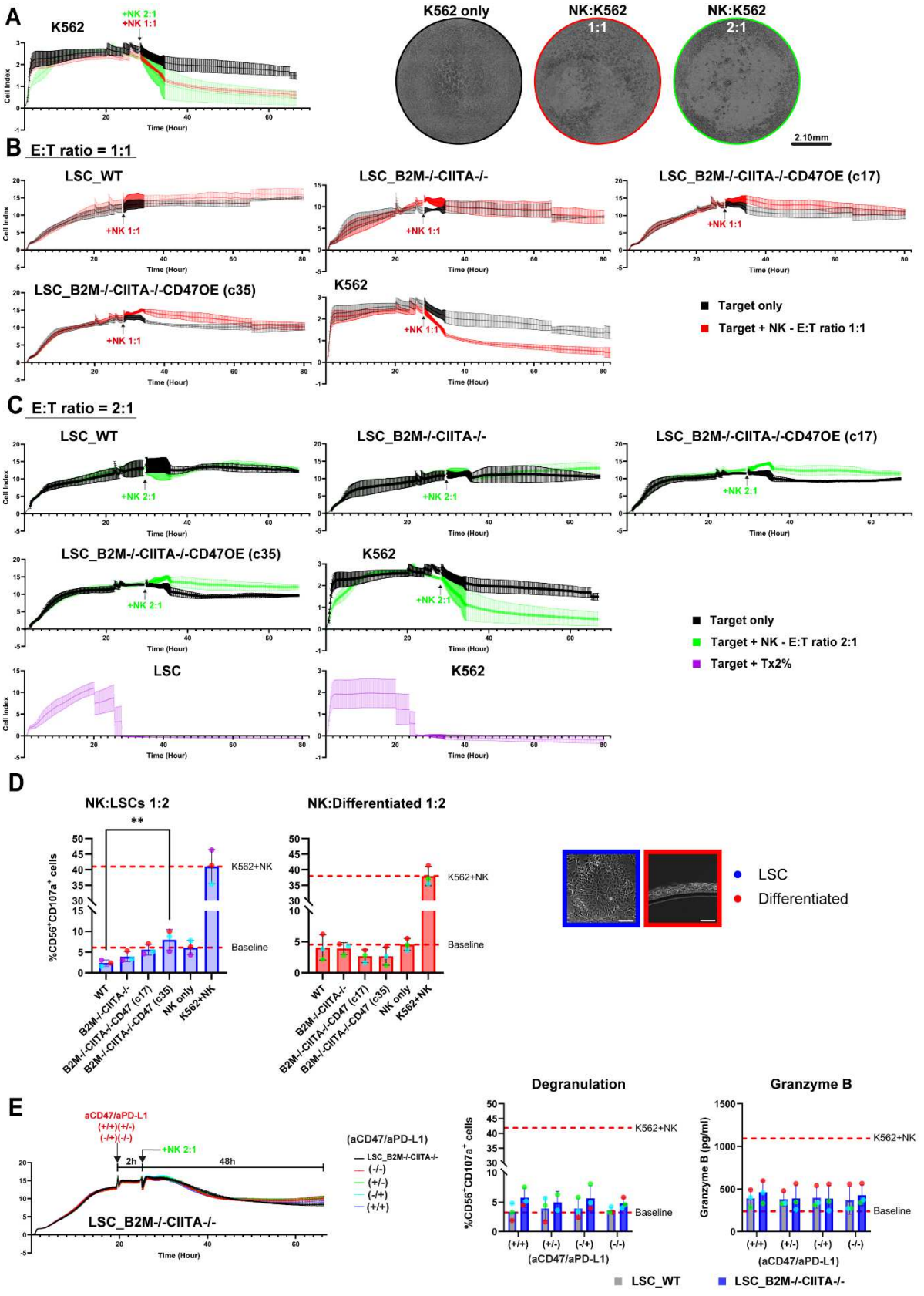
All panels: Data shown as mean ± *SD, (n=4)*. Statistical analysis was performed using one-way ANOVA with multiple comparisons followed by Tukey's multiple comparison test. * $p < 0.05$; ** $p < 0.01$; *** $p < 0.001$; **** $p < 0.0001$.


LSCs
Differentiated
WT
B2M-/-CIITA-/-
B2M-/-CIITA-/-CD47 (c17)
B2M-/-CIITA-/-CD47 (c35)
+aCD47
A
B
C
D
E
F
G
H
I
J
Normalised Total Orange Object Area (µm²/Image)
Elapsed time (h)
AUC
pHrodo® Red
+aCD47
+5µM CytD
WT
B2M-/-CIITA-/-
B2M-/-CIITA-/-CD47 (c17)
B2M-/-CIITA-/-CD47 (c35)

1597

Figure 6: CD47 overexpression protects *B2M*$^{-/-}$*CIITA*$^{-/-}$ LSCs and their ALI-differentiated derivatives from macrophage-mediated phagocytosis. (A) Time-lapse quantification of macrophage phagocytosis of pHrodo-Red-labelled LSCs. LSCs pretreated (**C**; n=3) or not pretreated (**B**; n=4) with anti-CD47 blocking antibody were co-incubated with monocyte-derived macrophages for 6 hours. **(D)** Area under the curve (AUC) of phagocytic activity from **(A)**, comparing pHrodo-Red+ signal between anti-CD47-treated and untreated LSCs over 6 hours. **(E)** Representative Incucyte snapshots of LSC phagocytosis at t = 3.5 hours. **(F)** Time-lapse quantification of macrophage phagocytosis of pHrodo-Red-labelled ALI-differentiated cells. Differentiated cells pretreated (**H**; n=3) or not pretreated (**G**; n=3) with anti-CD47 blocking antibody were co-incubated with monocyte-derived macrophages for 6 hours. **(I)** AUC of phagocytic activity from **(F)**, comparing pHrodo-Red+ signal between anti-CD47-treated and untreated LSCs over 6 hours. **(J)** Representative Incucyte snapshots of ALI-differentiated cell phagocytosis at t = 3.5 hours. For all snapshot panels, the first column represents the untreated condition, the second column the anti-CD47 antibody blocking condition, and the third column the phagocytosis-negative control in which macrophage activity was inhibited by cytochalasin D (5 µM). Images were acquired at 30-minute intervals using the Incucyte live-cell imaging system. Total orange object area of pHrodo-Red+ phagolysosomes per image was quantified as a measure of phagocytic activity. Data shown as mean ± SD.

Panels (D) & (I): Data shown as mean ± *SD*. Statistical analysis was performed using one-way ANOVA with multiple comparisons followed by Tukey's multiple comparison test. * $p < 0.05$; ** $p < 0.01$; *** $p < 0.001$; **** $p < 0.0001$.


A
K562
+NK 2:1
+NK 1:1
Cell Index
Time (Hour)
K562 only
NK:K562 1:1
NK:K562 2:1
2.10mm
B E:T ratio = 1:1
LSC_WT
LSC_B2M-/-CIITA-/-
LSC_B2M-/-CIITA-/-CD47OE (c17)
LSC_B2M-/-CIITA-/-CD47OE (c35)
K562
+NK 1:1
Target only
Target + NK - E:T ratio 1:1
C E:T ratio = 2:1
LSC_WT
LSC_B2M-/-CIITA-/-
LSC_B2M-/-CIITA-/-CD47OE (c17)
LSC_B2M-/-CIITA-/-CD47OE (c35)
K562
+NK 2:1
Target only
Target + NK - E:T ratio 2:1
Target + Tx2%
LSC
K562
D
NK:LSCs 1:2
NK:Differentiated 1:2
**
%CD56+CD107a+ cells
K562+NK
Baseline
WT
B2M-/-CIITA-/-
B2M-/-CIITA-/-CD47 (c17)
B2M-/-CIITA-/-CD47 (c35)
NK only
K562+NK
LSC
Differentiated
E
aCD47/aPD-L1
(+/+)(+/-)
(-/+)(-/-)
+NK 2:1
2h
48h
LSC_B2M-/-CIITA-/-
Time (Hour)
(aCD47/aPD-L1)
LSC_B2M-/-CIITA-/-
(-/-)
(+/-)
(-/+)
(+/+)
Degranulation
Granzyme B
%CD56+CD107a+ cells
Granzyme B (pg/ml)
K562+NK
Baseline
(+/+)
(+/-)
(-/+)
(-/-)
(aCD47/aPD-L1)
LSC_WT
LSC_B2M-/-CIITA-/-

1622

Figure 7: B2M$^{-/-}$CIITA$^{-/-}$ and B2M$^{-/-}$CIITA$^{-/-}$CD47OE LSCs resist NK cell-mediated cytotoxicity independently of CD47 and PD-L1. (A) xCELLigence real-time cell analysis (RTCA) of NK cell cytotoxicity against K562 cells used as HLA-I-deficient positive control **(B).** xCELLigence monitoring of NK cell cytolytic activity against WT, B2M$^{-/-}$CIITA$^{-/-}$, and B2M$^{-/-}$CIITA$^{-/-}$ CD47OE LSC clones co-cultured with allogeneic NK cells at an effector-to-target (E: T) ratio of 1:1 for 56 hours (n=5). **(C)** As in **(B)** at an E:T ratio of 2:1 for 48 hours (n=3). Data shown as mean ± SEM. **(D)** Flow cytometric quantification of NK cell degranulation, measured by CD107a surface expression, following co-culture with K562 cells, LSCs, and their ALI-differentiated derivatives across three independent NK cell donors. NK cells cultured alone served as baseline control (n=3). **(E)** Real-time xCELLigence monitoring of NK cell cytotoxicity against B2M$^{-/-}$CIITA$^{-/-}$ LSCs following pre-treatment with anti-CD47 and/or anti-PD-L1 blocking antibodies, with NK cell Fc receptors blocked before co-culture to minimise antibody-dependent cellular cytotoxicity (ADCC). Data shown as mean ± SEM. NK cell degranulation (CD107a) and granzyme B release were assessed in parallel for WT and B2M$^{-/-}$CIITA$^{-/-}$ LSC co-cultures (n=3). Data shown as mean ± SD.

Panel (D): Statistical analysis was performed using one-way ANOVA with multiple comparisons, followed by Tukey's multiple comparison test for. Panel (E): Statistical analysis was performed using multiple paired T test. * $p < 0.05$; ** $p < 0.01$; *** $p < 0.001$; **** $p < 0.0001$.

Supplementary Files

This is a list of supplementary files associated with this preprint. Click to download.

- SuplementaryTables.xlsx
- 1.SupplementaryMaterialSCRTdocx.docx
- 1.graphicalabstract.tif